Region- and activity-dependent regulation of extracellular glutamate in the brain

By

Nawrin Ferdous Pinky

A thesis submitted to the school of graduate studies in partial fulfilment of the requirements for the degree of Master of Science in Medicine (Neuroscience)

Faculty of Medicine

Memorial University of Newfoundland

October 2018

St John's **Newfoundland**

ABSTRACT

The rapid removal of synaptically-released glutamate is essential to maintain fast excitatory chemical neurotransmission and to prevent NMDA receptors mediated synaptic plasticity impairments and cell death. Here, we used the rapid extracellular fluorescent glutamate sensor, iGluSnFR (intensity-based glutamate sensing fluorescent reporter), and high-speed imaging to quantify relative differences in glutamate clearance rates over a wide range of presynaptic activity *in situ* in the hippocampus, cortex, striatum and cerebellum of male C57/BL6NCrl mice. We found that the hippocampus was significantly more efficient at clearing synaptically-released glutamate. We also found that pharmacological inhibition of GLT-1, the brain's most abundant glutamate transporter, slowed clearance rates to only ~ 20-25% of the effect induced by non-selective transporter blockade. In all, our data reveal clear regional differences in glutamate dynamics following neural activity and suggest that non-GLT-1 transporters can make a large contribution to the rate of glutamate clearance when GLT-1 is dysfunctional.

ACKNOWLEDGEMENTS

I would like to thank my supervisor, Dr. Matthew Parsons, for giving me the opportunity to fulfill my cherished dream to study neuroscience. I have been blessed with Dr. Parsons' guidance and motivation throughout the course of my Master's degree.

I am grateful to my lab mates for being so helpful and giving me the opportunity to enhance my learning.

I would like to thank my husband, Nahian, for being the most supportive and understanding person. I am ever thankful to my parents for being the amazing parents as they are.

I thank the members of my supervisory committee, Dr. Michiru Hirasawa and Dr. Jacqueline Vanderluit and my funding agency NSERC for their support.

-Nawrin Ferdous Pinky

TABLE OF CONTENTS

LIST OF TABLES

LIST OF FIGURES

LIST OF ABBREVIATIONS

ACSF: Artificial cerebrospinal fluid

AMPA: α-amino-3-hydroxyl-5-methyl-4-isoxazole-propionate

APS: Ammonium Persulfate

BSA: Bovine serum albumin

BME: Beta- mercaptoethanol

CaMKII: Ca^{2+}/calmodulin-dependent protein kinase II

CNS: Central nervous system

CSF: Cerebrospinal fluid

D: Day

D-AP5: D-(-)-2-Amino-5-phosphonopentanoic acid

DHK: Dihydrokainic acid

DL-TBOA: DL-threo-β-Benzyloxyaspartic acid

DNQX disodium salt: 6,7-Dinitroquinoxaline-2,3-dione disodium salt

EAAC1: excitatory amino acid carrier 1

EAAT1: Excitatory amino acid transporter 1

EAAT2: Excitatory amino acid transporter 2

EAAT3: Excitatory amino acid transporter 3

EAAT4: Excitatory amino acid transporter 4

EAAT5: Excitatory amino acid transporter 5

EPSC: Excitatory postsynaptic currents

F/F: Fluorescence/ fluorescence

GFAP: Glial fibrillary acidic protein

GFP: Green fluorescent protein

GLT-1: Glutamate transporter-1

GLAST: Glutamate aspartate transporter

HFS: High frequency stimulation

Hz: Hertz

iGluSnFR: Intensity-based glutamate sensing fluorescent reporter

IOS: Intrinsic Optical signal

KAR: Kainate receptors

LED: Light-emitting diode

mGluR: metabotropic glutamate receptor

min: minute

NMDA: *N*-methyl-D-aspartate

NMDAR: *N*-methyl-D-aspartate receptor

ROI: region of interest

RM Anova: Repeated measure anova

STC: Synaptically-activated transporter current

SEM: Standard Error of Mean

SLC1A1: Solute carrier family 1, member 1

SLC1A2: Solute carrier family 1, member 2

SLC1A3: Solute carrier family 1, member 3

SLC1A6: Solute carrier family 1, member 6

SLC1A7: Solute carrier family 1, member 7

TTL: Transistor-to-transistor logic

V: Volt

v/v: volume to volume

VSD: voltage sensitive dye

VGLUT: vesicular glutamate transporters

CO-AUTHORSHIP STATEMENT

Most of the research presented in this thesis has been published in-

Journal of Neuroscience 6 June 2018;

DOI: https://doi.org/10.1523/JNEUROSCI.3213-17.2018

Pubmed: 29760178

As-

Region- and Activity-Dependent Regulation of Extracellular Glutamate

Nawrin F. Pinky, Crystal M. Wilkie, Jocelyn R. Barnes and Matthew P. Parsons

I, Nawrin Ferdous Pinky, am the first author of the manuscript. All the experiments except the western blot experiment for Figure A1 in the appendix was done by me. Crystal Wilkie performed the western blot experiments. Jocelyn Barnes contributed to the experiments required for the revision of the manuscript, which do not appear in this thesis. My Supervisor, Dr. Matthew Parsons guided me throughout the experiment and writing process.

Chapter 1 – Introduction

The neurotransmitter glutamate is required for rapid cellular communication, cell survival and many forms of synaptic plasticity**.** However, if too much glutamate accumulates in the extracellular space, it can impair synaptic plasticity and trigger apoptotic cell death (Danbolt 2001). Glutamate toxicity contributes to neuronal death in a variety of neurodegenerative diseases, including Huntington disease, Alzheimer disease and Amyotrophic Lateral Sclerosis (Hynd, Scott, & Dodd 2004; Milnerwood et al., 2010; Parsons & Raymond, 2014; Van Den Bosch, Van Damme, Bogaert, & Robberecht, 2006). Thus, understanding how the healthy brain efficiently clears extracellular glutamate during times of heightened neural activity may help us better understand disease states associated with glutamate toxicity. While different brain regions show dramatically different responses to plasticity-inducing neural activity as well as different susceptibility to glutamate toxicity, whether regional differences exist in glutamate clearance capacity is poorly understood. My study focused on the real-time extracellular glutamate dynamics in 4 different brain regions (hippocampus, cortex, striatum and cerebellum), each of which receive dense glutamatergic innervation.

1.1 Glutamate: the brain's most abundant excitatory neurotransmitter

L-Glutamate, an amino acid, is the most abundant excitatory neurotransmitter in the mammalian brain. Glutamate is essential for fast excitatory neurotransmission and plays a key role in cognition, learning and memory (Danbolt 2001; Fonnum, 1984; O P

Ottersen & Storm-Mathisen, 1984). By recording the membrane potential from motor neurons in response to exogenous glutamate application, it was first demonstrated in the 1950s that glutamate has an excitatory effect in the central nervous system (CNS) (Curtis, Lodge, & McLennan, 1979; Curtis, Phillis, & Watkins 1961). In the late 60s and early 70s, several studies demonstrated that glutamate is synthesized in presynaptic terminals and that, upon physiologically-relevant stimulation patterns, can be released in sufficiently high amounts to exert a postsynaptic response, thereby meeting all the criteria of neurotransmitter (Curtis & Johnston, 1974; Fonnum, 1984). Glutamate is now recognized as the principal excitatory neurotransmitter in the vertebrate nervous system, and has been since the early 1970s (Meldrum, 2000).

Extracellular glutamate concentrations vary widely and can range from nanomolar (in the absence of neural activity) to millimolar (during neural activity) concentrations (Bergles & Jahr 1997; Clements, 1996; Diamond & Jahr 1997). At rest, dramatic differences in glutamate concentration are observed, with nerve terminal concentrations typically being a thousand-fold greater than in the extracellular space (Danbolt 2001; O. P. Ottersen, Zhang, & Walberg, 1992; O. P. Ottersen, Laake, Reichelt, Haun, & Torp 1996). Neural activity results in a rapid and localized increase in the extracellular glutamate concentration from the nanomolar to millimolar range (Dzubay & Jahr, 1999); the localized and transient nature of extracellular glutamate fluctuations has complicated experimental measurements of glutamate concentrations. For example, *in vitro* (electrophysiology) and *in vivo* (microdialysis or voltammetry) studies of extracellular glutamate concentration has shown a variance in glutamate concentration

ranging from 0.02–0.1μM (measured by electrophysiology; (Herman & Jahr, 2007) to 1–30μM (measured by microdialysis and voltammetry; (Day, Pomerleau, Burmeister, Huettl, & Gerhardt, 2006; McLamore et al., 2010; Moussawi, Riegel, Nair, & Kalivas, 2011; Oldenziel et al., 2007) with the majority of microdialysis measurements falling in the 1-5 μM range (Baker et al., 2003; Melendez, Hicks, Cagle, & Kalivas, 2005; Miele, Berners, Boutelle, Kusakabe, & Fillenz, 1996; Miller et al., 2008). These discrepancies likely reflect the transient nature of glutamate neurotransmission; localized glutamate concentrations can fluctuate from the nanomolar to millimolar range on a millisecond timescale during neural activity (Bergles & Jahr 1997).

1.1.1 Essential components of glutamatergic neurotransmission: release, receptor, reuptake, recycle

In the nerve terminal, glutamate is transported into synaptic vesicles by vesicular glutamate transporters (VGLUTs: VGLUT 1, VGLUT 2, VGLUT 3) (Liguz-Lecznar & Skangiel-Kramska, 2007; Naito & Ueda, 1983). Glutamate is released from the presynaptic glutamate-containing vesicles into the extracellular space via exocytosis (Cousin & Robinson, 1999; Ludger & Galli, 1998). During neural activity, glutamate is released into the synaptic cleft, where it can bind with different classes of glutamate receptors. Glutamate receptors are divided into ionotropic and metabotropic subtypes, which can localize to both pre- and postsynaptic membranes (Backus, Kettenmann, & Schachner, 1989; Glaum, Holzwarth, & Miller, 1990; Grewer & Rauen, 2005; Nakanishi et al., 1994; Sontheimer, Kettenmann, Backus, & Schachner, 1988). Ionotropic glutamate receptors directly convert the chemical signal into an electrical response. In contrast,

metabotropic glutamate receptors act indirectly through second messenger systems which can exert a wide variety of downstream effects (Nakanishi et al., 1994).

Ionotropic and metabotropic glutamate receptors can be further broken down into different subtypes. The families of ionotropic glutamate receptor include α-amino-3-hydroxyl-5-methyl-4-isoxazole-propionate (AMPA) / Kainate receptors and *N*-methyl-D-aspartate (NMDA) receptors. Metabotropic receptors (mGluR1-8) are subdivided into three groups based on sequence homology: group I (mGluR1, mGluR5), group II (mGluR2 and mGluR3) and group III (mGluR4, mGluR6, mGluR7, mGluR8). Group I mGluRs are located mainly post-synaptically and enhance neuronal excitability, whereas group II and III mGluRs are mainly presynaptic and inhibit neurotransmitter release (Niswender & Conn, 2010). AMPA receptors (AMPARs) and kainite receptors (KARs) can be further divided into subgroups based on their subunit composition: GluA1- GluA4 subunits for AMPARs and GluK1- GluK5 subunits for KARs (Traynelis et al., 2010).

AMPARs are heterotetrameric complexes (Song & Huganir, 2002) that assemble from four distinct subunits; interestingly, AMPAR subunit composition determines the Ca^{2+} permeability of the receptor (Greger, Ziff, & Penn, 2007). AMPARs are typically permeable to cations Na^{+} and K^{+}, and Ca^{2+} ion flux is prevented by the presence of the GluA2 subunit. However, AMPARs lacking the GluA2 subunit are fully functional and permeable to Ca^{2+} (Meldrum, 2000). AMPARs have rapid activation and inactivation kinetics, with AMPAR-mediated excitatory postsynaptic currents (EPSCs) decaying within a few milliseconds (Clements, Feltz, Sahara, & Westbrook, 1998; Colquhoun,

Jonas, & Sakmann, 1992; Hestrin, 1992). AMPAR-mediated EPSCs represent the primary contributor to rapid postsynaptic current flux at a typical excitatory synapse (Meldrum, 2000).

NMDA receptors (NMDARs) play an important role in synaptic transmission and neural plasticity during learning and memory due to their unique characteristics, including their slow activation kinetics (occurring in ~10 ms) (Dzubay & Jahr, 1996), slow inactivation kinetics, high permeability to Ca^{2+} and blockade by Mg^{2+} at resting membrane potentials. Activation of NMDARs require not only glutamate binding, but also the removal of the Mg^{2+} block by postsynaptic depolarization, as well as the binding of the co-agonist glycine or D-serine (Dore et al., 2017; Iacobucci & Popescu, 2017; Traynelis et al., 2010). In this regard, NMDARs act as "coincidence detectors" in that they require simultaneous presynaptic release and postsynaptic depolarization for their activation. NMDARs have slower activation kinetics compared to AMPARs and have a higher affinity for glutamate (Traynelis et al., 2010); this high affinity, in addition to the slow inactivation kinetics, contributes to the long duration of NMDAR-mediated EPSCs (Lester & Jahr, 1992). The Ca^{2+} permeability of NMDARs plays a crucial role in synaptic plasticity by activating a variety of kinases and/or phosphatases such as Ca^{2+}/calmodulin-dependent protein kinase II (CaMKII) and calcineurin (Song & Huganir, 2002). Structurally, NMDARs are heterotetramers consisting of an obligatory GluN1 subunit and a combination of GluN2A-D and/or GluN3A-B subunits (Traynelis et al., 2010). The heterogeneous composition of NMDARs is responsible for the observed diversity in NMDAR function including its kinetics, sensitivity to magnesium, permeability to

calcium, and association with various downstream signaling pathways. As an example, the decay time of NMDAR-mediated EPSCs can vary within a 50-fold range depending upon the GluN2 subunit present, with GluN1/GluN2A-containing NMDARs producing the fastest decay kinetics and GluN1/GluN2D-containing NMDARs producing the slowest decay kinetics (Paoletti, Bellone, & Zhou, 2013; Vicini et al., 1998).

In addition to the NMDAR functional diversity resulting from subunit differences, the consequences of NMDAR activation also depend heavily on the duration and the subcellular localization of the activated receptor. Synaptically located NMDARs are predominantly GluN2A-containing, whereas perisynaptic and extrasynaptic sites are enriched with GluN2B-containing NMDARs (Gladding & Raymond, 2011; Hardingham & Bading, 2010; Parsons & Raymond, 2014). Therefore, the rate by which glutamate is cleared from the extracellular space following neural activity can dramatically affect NMDAR signaling.

The spatiotemporal profile of extracellular glutamate during neural activity shapes the fate of NMDAR-mediated transmission. While a brief and localized change in glutamate concentration results in phasic NMDAR-mediated synaptic transmission, the sharp rise in extracellular glutamate must be cleared quickly in order to avoid excessive activation of extrasynaptic NMDARs. It is the responsibility of the glutamate uptake system to maintain the basal extracellular concentration of glutamate at a low nanomolar range to minimize NMDAR activity at rest (Vyklicky et al., 2014)**.** It is essential for the brain to maintain a low level of tonic extracellular glutamate in order to achieve a high

signal-to-noise ratio during synaptic transmission, and to prevent glutamate from reaching excitotoxic concentrations (Danbolt 2001; Parsons & Raymond, 2014) . It has been postulated that the activation of GluN2A-containing NMDARs in the synaptic region promotes cell survival and synaptic plasticity, while the activation of GluN2B-containing NMDARs in the extrasynaptic region promotes synapse weakening and excitotoxic cell death. There are no enzymes present that can degrade extracellular glutamate; therefore, cellular uptake is the only mechanism that exists to remove glutamate from the extracellular space and prevent the over-activation of cell death-associated extrasynaptic NMDARs (Balcar & Johnston, 1972; Danbolt 2001). Glutamate transporters are required for the cellular uptake of glutamate, and therefore mediate the spatiotemporal dynamics of glutamatergic neurotransmission (Tzingounis & Wadiche, 2007; Y. Zhou & Danbolt, 2014).

1.2 Glutamate transporters

Astrocytes play an essential role in the rapid recycling of glutamate from the extracellular space. Glutamate that is taken up through glutamate transporters located on astrocytes is recycled and then reused as a neurotransmitter in the nerve terminal, through a process known as the "glutamate-glutamine cycle". In astrocytes, glutamate is converted into glutamine by the enzyme glutamine synthetase, and released into the extracellular space where it is taken up by nerve terminals and converted back to glutamate (Danbolt 2001; Grewer & Rauen, 2005; Y. Zhou & Danbolt, 2014). This cycle is crucial to the maintenance of glutamatergic neurotransmission. Therefore, transporters

play the dual role of maintaining low extracellular glutamate level and recycling glutamate.

1.2.1 Glutamate transporter subtypes

Glutamate transporters are membrane-bound proteins that are responsible for the cellular uptake of glutamate. In doing so, glutamate transporters play a crucial role in shaping the dynamics of synaptic neurotransmission on a millisecond time scale (Diamond & Jahr 1997). There are five known sodium-dependent glutamate transporters, the location of which varies greatly from one brain region to the next. The most abundant glutamate transporter, glutamate transporter-1 (GLT-1, *SLC1A2* also known as excitatory amino acid transporter 2, or EAAT2), is highly expressed in astrocytes throughout the neuroaxis, with particularly high expression levels observed in the hippocampus and neocortex (Danbolt, Storm-Mathisen, & Kanner 1992; Levy, Lehre, Rolstad, & Danbolt, 1993). The glutamate aspartate transporter (GLAST; *SLC1A3* also known as excitatory amino acid transporter 1, or EAAT1) is also present in astrocytes throughout the CNS, and is particularly enriched in the cerebellum (Berger & Hediger, 1998; Ginsberg, Martin, & Rothstein, 1995; Lehre, Levy, Ottersen, Storm-Mathisen, & Danbolt, 1995; Rothstein, Van Kammen, Levey, Martin, & Kuncl 1995; Schmitt, Asan, Pü, & Kugler, 1997). Both GLAST/EAAT1 and GLT-1/EAAT2 are abundantly expressed in the plasma membrane of astrocytes, with a subcellular localization that results in a high transporter density near axon terminals. In contrast, excitatory amino acid transporters 3 and 4 (EAAT3 and EAAT4, respectively) are predominantly expressed in neuronal membranes, with little-to-

no expression found in astrocytes (Holmseth et al., 2012; Kanai & Hediger, 1992; Rothstein et al. 1994; Shashidharan et al., 1997). EAAT3 (*SLC1A1*) is expressed in neurons throughout the CNS, while EAAT4 (*SLC1A6*) is predominantly found in dendritic spines in the cerebellum. Excitatory amino acid transporter 5 (EAAT5; *SLC1A7*) expression in the brain is very low and found predominantly in the retina (Dehnes et al., 1998; Fairman, Vandenberg, Arriza, Kavanaught, & Amara, 1995). Table 1 below summarizes both the cellular and regional locations of the glutamate transporter subtypes:

Glutamate transporter	Regional location	Cellular location
EAAT 1/ GLAST	In all brain areas, highest in cerebellum	Astrocytes
EAAT2/ GLT-1	In all brain areas, highest in hippocampus and neocortex (layer I-VI)	Astrocytes
EAAT 3/ EAAC1	Throughout CNS, mainly hippocampus	Neurons
EAAT 4	Predominantly in Cerebellar Purkinje cells	Neurons
EAAT 5	Retina	Retinal photoreceptors and bipolar cells

Table 1: Regional and cellular locations of the different excitatory amino acid transporter (EAAT) subtypes. Adapted from Yun Zhou & Danbolt, 2013

1.2.2 Knockout studies: uncovering the role of individual glutamate transporters

The first glutamate transporter to be purified was GLT-1 (Danbolt, Pines, & Kanner 1990; Pines et al. 1992). Early studies indicated that GLT-1 is responsible for approximately 95% of glutamate uptake activity (Danbolt et al. 1992; Haugeto et al., 1996), a number that is still highly-cited today. In mice, genetic deletion of the *SLC1A2* gene that encodes the GLT-1 protein confirmed an essential role for GLT-1 in maintaining a low concentration of extracellular glutamate and protecting the brain from excitotoxicity (Otis & Kavanaugh, 2000; Tanaka et al., 1997). GLT-1 deficient homozygous mice present with epilepsy, an increased susceptibility to acute cortical injury and a reduced life span. Knocking out GLAST and GLT-1 together results in perinatal mortality (Kiryk, Aida, Tanaka, & Banerjee, 2008; Matsugami et al., 2006; Otis & Kavanaugh, 2000; Tanaka et al., 1997). GLAST deficient mice exhibit impaired cerebellar function, resulting in poor motor coordination (Watase et al., 1998). Genetic deletion of EAAT3 in mice results in premature aging as determined by age dependent brain atrophy (cortical thinning and ventricular enlargement), and pronounced behavioral abnormalities including a reduction in spontaneous locomotor activity (Aoyama et al., 2006; Lane et al., 2014; Stoffel, 1997).

1.2.3 Mechanism of glutamate transport

The glutamate transporters are commonly referred to as "high affinity transporters" due to their high affinity for glutamate. The Kt values for GLAST, GLT-1 and EAAC1 ranges between 10-20 μM of glutamate (Tzingounis & Wadiche, 2007). The affinities for EAAT4 and EAAT5 are of higher and lower magnitude by one order, respectively (Arriza et al., 1994; Danbolt 2001; Fairman et al., 1995). It is important to note that the effective transport of glutamate during neural activity depends not only upon the affinity of the transporters, but also the probability of successful transport upon glutamate binding, the time required to complete a transport cycle (i.e. turnover rate), and the subcellular localization of the transporter expression with respect to the sites of glutamate release (Tzingounis & Wadiche, 2007; Vandenberg & Ryan, 2013; Zhou & Danbolt 2014). The stoichiometry of glutamate transport couples the co-transport of one glutamate molecule with three Na^+ ions and one H^+ ion from outside to inside the cell, with the movement of one K^+ ion from inside to outside of the cell (Figure 1) (Zhou & Danbolt 2013). In addition, EAAT4 and EAAT5 exhibit a non stoichiometrically-coupled glutamate-gated Cl^- current conductance, thereby acting as an extracellular glutamate sensor that can induce cellular hyperpolarization (Fairman et al. 1995; Melzer, Torres-Salazar, & Fahlke, 2005; Veruki, Mørkve, & Hartveit, 2006; Wadiche, Amara, & Kavanaugh, 1995).

Glutamate transporters are homomers composed of three independent subunits (homotrimers) in the shape of a bowl, with the glutamate binding site located towards the bottom of the bowl and in between two hairpin loops of gates to the glutamate binding

site (Grewer & Rauen, 2005; Tzingounis & Wadiche, 2007; Yernool, Boudker, Jin, & Gouaux, 2004). Glutamate transporters have two major conformations: an outward conformation with the glutamate binding site exposed to the extracellular space, and an inward conformation with the glutamate binding domain exposed to the cytoplasm. When glutamate and co-transported ions sequentially bind with the outward conformation, it leads to translocation of the amino acid to the inside, whereas binding of an intracellular K^+ ion to the inward conformation leads to the reorientation of the glutamate binding site, back to the outward state.

1.2.4 Developmental regulation of glutamate transporters

The contribution of glutamate transporters to the rate of glutamate clearance from the extracellular space gradually increases with development. Low glial transporter expression results in slow transporter-mediated uptake in the neonatal rat brain in the first week of life. As neural circuitry matures, transporter expression increases and reaches adult levels by about one month of age (Schmidt, Wolf, & Republic, 1988; Thomas, Tian, & Diamond 2011; Ullensvang, Lehre, & Danbolt, 1997). Interestingly, in the rat brain, GLAST expression is initially higher than GLT-1 during early postnatal development, but the density of GLT-1 rapidly increases and by one month of age, GLT-1 becomes the predominant glutamate transporter in the CNS (Christensen & Fonnum, 1992; Kish, Kim, & Ueda, 1989; Matsugami et al., 2006; Ullensvang et al., 1997).

While the aforementioned developmental studies were largely conducted in the hippocampus, the early increase in glutamate transporter expression is also readily observed in additional brain regions. Electrophysiological recordings of synaptically-

activated transporter currents (STCs) demonstrate that that the efficiency of glutamate uptake increases with age in both the hippocampus and cortex (Hanson et al., 2015).

1.3 Role of diffusion in glutamate clearance

Following neural activity and the synaptic release of glutamate, in addition to transporter-mediated uptake, the extracellular concentration of glutamate at a given location can also be reduced by passive diffusion. Therefore, overall extracellular glutamate dynamics will depend on the transporter localization and density, as well as the geometry and barriers present in the local extracellular microenvironment (Sarantis et al., 1993).

Diffusion rate is dependent upon the structure of the extracellular space. The two factors that affect the extracellular diffusion rate are volume fraction and tortuosity (Nicholson & Sykova, 1998). Tortuosity refers to barriers to diffusion and is quantified by comparing diffusion in the sample of interest to the diffusion of the same substance in a free medium. Volume fraction simply refers to the volume of extracellular (void) space (Nicholson & Sykova, 1998). The geometry of the extracellular matrix, largely shaped by glial cells, contributes to the tortuosity (Nicholson, Kamali-Zare, & Tao 2011). Methods such as real-time iontophoresis and integrative optical imaging have shown, not surprisingly, that narrow and tortuous space slows diffusion across the extracellular space (Nicholson & Tao, 1993; Syková, Nicholson, & Sykova, Eva; Nicholson, 2008). Interestingly, electron microscopy studies have demonstrated that as glutamate transporter expression increases during development, the volume of the extracellular decreases,

resulting in a shift from fast diffusion and slow uptake in the neonate brain, to slow diffusion and rapid uptake in the adult brain (Thomas et al. 2011). The contribution of diffusion to glutamate clearance cannot be measured by the biochemical uptake assay, and it has been difficult to ascertain how much diffusion contributes to the kinetics of the STC.

1.4.1 Quantifying the efficiency of glutamate uptake with the biochemical uptake assay

Soon after glutamate was identified as the primary excitatory neurotransmitter in the CNS, it was recognized that novel methods would be required to study how the spatial and temporal dynamics of this essential signaling molecule were regulated. Several technological approaches were established to quantify the efficiency of high-affinity glutamate uptake. Among them, the biochemical uptake assay has dramatically increased out understanding of the glutamate transporter system, and is still in heavy use today (Currie & Kelly, 1981; Danbolt, Furness, & Zhou 2016).

The biochemical uptake assay is often performed in neuronal and/or astrocyte cultures from different brain regions (such as hippocampus, cortex, striatum, cerebellum) (Horak, Nashner, & Diener, 1990) or using synaptosomal preparations (pinched off nerve-endings; Danbolt et al. 2016; Dodd et al., 1981; Morgan, 1971; Raiteri & Raiteri, 2000). In this assay, the culture medium or the synaptosome homogenate is incubated in a known concentration of exogenous, radio-labeled glutamate for several minutes. Liquid

scintillation is then used to quantify the glutamate uptake capacity of the preparation (Levi & Raiteri, 1973). Although this biochemical assay is a commonly used preparation that is still widely used today, it is associated with some important caveats. While the majority of glutamate transporters are expressed on astrocyte membranes, so-called "pure" synaptosomal preparations should contain little-to-no astrocytes, and the purity of a synaptosome preparation is likely to vary greatly from one lab to another. Indeed, a recent study demonstrated that the biochemical uptake assay grossly overemphasizes the contribution of neuronal uptake to total glutamate transport (Petr et al., 2015). In addition, the biochemical assay is unable to mimic the physiological properties of synaptic release, and is devoid of any tripartite synaptic structure, factors that undoubtedly contribute to the extracellular profile of glutamate transients (Danbolt et al. 2016). Overall, biochemical assays lack the representation of physiological glutamate dynamics *in situ*, and it has been suggested that glutamate uptake should be studied *in situ* wherever possible (Danbolt et al. 2016; Danbolt 2001; Petr et al., 2015).

1.4.2 Quantifying the efficiency of glutamate uptake with electrophysiological measures of transporter currents

To increase our fundamental understanding of glutamate transport, it is necessary to quantify the clearance rates of endogenous glutamate *in situ* following synaptic activity. Glutamate transport is an electrogenic process; there is net influx of positive charge associated with each transport cycle (Brew & Attwell, 1987; Schwartz & Tachibana, 1990; Wyllie, Mathie, Symonds, & Cull- Candy, 1991). The electrogenic

nature of glutamate uptake enables its quantification using whole-cell electrophysiology. By measuring this electrogenic transporter current in astrocytes via patch-clamp recording, it is possible to determine the contribution of glutamate transporters to the clearance of synaptically-released glutamate. Interestingly, while STCs are typically measured in astrocytes (Bergles & Jahr 1997) they have also been observed in neurons (Otis, Kavanaugh, & Jahr, 1997 1997), reflecting the expression of glutamate transporters on both cell types. However, STC measurements are almost always made from astrocytes because of the high density of glutamate transporters on astrocyte membranes. STC in glial cells has been measured in culture (Linden, 1997), and acute slices from different brain regions including the cerebellum (Clark & Barbour, 1997), hippocampus (Bergles & Jahr 1997), cortex (Armbruster, Hampton, Yang, & Dulla, 2014; Armbruster, Hanson, & Dulla, 2016; Hanson et al., 2015) and striatum (Parsons et al., 2016). Nonetheless, STC recordings are technically demanding, are extremely difficult to elicit in brain regions with relatively weak glutamatergic afferent connectivity, and are restricted to the glutamate profile occurring at a single astrocyte. Furthermore, using STCs to understand how extracellular glutamate profiles are influenced by transporter dysfunction is complicated by the fact that transporter inhibition/dysfunction will reduce the size of the STC itself to undetectable levels.

1.4.3 Using novel iGluSnFR technique to revisit extracellular glutamate dynamics

Despite the extremely organized morphology of tripartite synaptic structure (Perea, Navarrete, & Araque, 2009), with the exception of electrophysiological recordings

of STCs, the large majority of our knowledge of glutamate transporter function has been derived from biochemical uptake assays in homogenized tissue preparations. While it is widely accepted that astrocytes mediate the bulk of glutamate uptake in the brain, the biochemical uptake assay was recently shown to dramatically overemphasize neuronal uptake at the expense of astrocytic uptake, highlighting the need to study glutamate dynamics and glutamate transporter function *in situ* (Petr et al., 2015). Optogenetics provides us with a relatively new biosensor to study glutamate dynamics, allowing for the real-time visualization and quantification of glutamate dynamics *in situ*. The extracellular glutamate sensor called iGluSnFR (intensity based glutamate sensing fluorescent reporter) opened a new window to study glutamate dynamics in real-time (Marvin et al., 2013). iGluSnFR is a circular GFP molecule which is fused to an extracellular glutamate binding site. When glutamate is not bound with the iGluSnFR, the GFP fluoresces at a low intensity. When glutamate binds with iGluSnFR, it causes conformational changes in the iGluSnFR molecule and the GFP intensity increases. The whole process occurs on a millisecond time scale and is highly selective to extracellular glutamate. These features make iGluSnFR a perfect candidate to measure glutamate clearance *in situ*. In this thesis, I use iGluSnFR to understand how glutamate dynamics are influenced by different brain regions and in response to varying degrees of neural activity.

1.5 Hypothesis

Glutamate clearances rates vary in both a region- and activity-dependent manner; thus, glutamate uptake should be studied in real-time, *in situ* and in response to endogenous glutamate release during neural activity.

1.6 Aims of the thesis project

- Use iGluSnFR to visualize, in real-time, the spatiotemporal extracellular dynamics of synaptically-released glutamate over a wide range of presynaptic activity in the hippocampus, cortex, striatum and cerebellum.
- Use a pharmacological approach to quantify the contribution of GLT-1 and non-GLT-1 glutamate transporters to the overall clearance rates of synaptically-released glutamate in hippocampus, cortex, striatum and cerebellum.

Chapter 2: Materials and Methods

2.1 Animals

All experiments were performed on acute brain slices obtained from male C57BL/6NCrl mice. Mice were ordered from Charles River at ~3–4 weeks of age and were provided with a minimum of 2 d of acclimatization upon arriving at Memorial University's animal care facility. Mice were group housed in ventilated cage racks, were provided with standard chow and water *ad libitum*, and were maintained on a normal 12 hours light/dark cycle. All experimental procedures were approved by Memorial University's Institutional Animal Care Committee and were performed in accordance with the guidelines set by the Canadian Council on Animal Care.

2.2 Stereotaxic surgery

Male C57BL/6NCrl mice (4–6 weeks of age) were anesthetized by isoflurane inhalation (3%) and maintained with 1.5–2% isoflurane for the duration of the surgical procedure. Mice were placed on a heating pad to maintain body temperature throughout the surgery and secured within the ear bars of a standard stereotaxic apparatus (Stoelting). Eye drops were used to lubricate the eyes throughout the procedure, and a subcutaneous 0.5 ml injection of 0.9% sterile saline was provided to help prevent dehydration. When unresponsive to toe-pinch, a small amount of fur above the scalp was cut with a pair of scissors, and a 0.1 ml bolus of 0.2% lidocaine was injected below the scalp. A small incision was then made in the scalp around bregma, and the underlying skull was

exposed. A hand drill was used to carefully thin the skull at the desired coordinates from bregma, and a fine bent needle tip was used to peel back the last layer of skull to expose the underlying cortex while minimizing tissue damage. A Neuros 7002 Hamilton syringe was attached to an infusion pump (Pump 11 Elite Nanomite; Harvard Apparatus, Massachusetts, United States), which was then secured to the stereotaxic frame. A total volume of 1 µl of AAV1.hSyn. iGluSnFr.WPRE.SV40 (synapsin-iGluSnFR; Penn Vector Core, catalog #AV-1-PV2723; kindly provided by Dr. Loren L. Looger and Janelia Research Campus of the Howard Hughes Medical Institute, Ashburn, VA) was injected into the hippocampus, cortex, striatum or cerebellum at an injection rate of 2 nl/s. The syringe was left in place for an additional 5 min after the injection. The following coordinates were used with respect to bregma: hippocampus, 2.6 mm posterior, 2.4 mm lateral (right), 1.9 mm ventral to brain surface; cortex, 0.7 mm anterior, 2.0 mm lateral (right), 0.6 mm ventral; striatum, 0.7 mm anterior, 2.0 mm lateral (right), 2.6 mm ventral; cerebellum- 2.6 mm posterior, 2.00 mm right lateral, 1.00 mm ventral to brain surface. The syringe was slowly withdrawn, the incision was sutured, and mice were given a subcutaneous injection of 0.5 ml of 0.9% saline containing 2 mg/kg meloxicam before being placed on a heating pad for ~30 min to accelerate recovery.

2.3 Slice preparation

At 2–3 months of age (3–6 weeks after iGluSnFR injection to ensure proper expression of the virus within the injected brain region), mice were anesthetized with isoflurane and decapitated, and the brain was quickly removed and immersed in ice-cold oxygenated

(95% O2/5% CO2) slicing solution consisting of (in mM) 125 NaCl, 2.5 KCl, 25 NaHCO3, 1.25 NaH2PO4, 2.5 MgCl2, 0.5 CaCl2, and 10 glucose.

Coronal brain slices (350 μm) containing the hippocampus, striatum, cortex or cerebellum were obtained with a Lecia VT1000 Vibratome (Greenville, USA). Slices were then placed in artificial cerebrospinal fluid (ACSF) containing (in mM) 125 NaCl, 2.5 KCl, 25 NaHCO3, 1.25 NaH2PO4, 1 MgCl2, 2 CaCl2, and 10 glucose. Slices were recovered in oxygenated ACSF for 45 min at room temperature before experimentation.

2.4 Imaging and image analysis

Slices were then transferred to the recording chamber, and a peristaltic pump (MP-II; Harvard Apparatus) was used to perfuse oxygenated ACSF at a flow rate of 2 ml/min. ACSF was heated to 32°C using an in-line heater and temperature controller (TC- 344C; Harvard Apparatus). Glass stimulating electrodes were pulled using a Narishige PB-7 pipette puller to a resistance of 1–3MΩ when filled with ACSF. For hippocampal sections, the stimulating electrode was placed directly in the Schaffer collateral pathway within the stratum radiatum. For cortical sections, the stimulating electrode was placed in the deep layers of the somatosensory cortex. For striatal sections, the stimulation electrode was placed in the dorsal striatum. For the cerebellar slices, the glass electrodes were placed in the molecular layers of the cerebellum. In all cases, the stimulating electrode was placed at a depth ~50–100 μm below the slice surface. Clampex software (Molecular Devices, San Jose, California, USA) was used to send TTL triggers through the digital outputs of a Digidata 1550A (Molecular Devices) for precise control over an

LED illumination source (Prior, Lumen 300), an EM-CCD camera (Andor, iXon Ultra 897), and an Iso-flex stimulus isolator (AMPI). A basal, unstimulated iGluSnFR expression level was first measured in each slice using a constant LED power and exposure time. iGluSnFR responses to evoked neural activity were recorded with Andor Solis software, using 4 x 4 binning and an acquisition rate of 205 frames per second. Evoked iGluSnFR responses were averaged over three to five trials, with nonstimulus trials interleaved to control for any bleaching of the iGluSnFR signal during acquisition. The nonstimulus trials were averaged in ImageJ (https://imagej.nih.gov/ij/) and subtracted from the average of the stimulus trials using the IOS and VSD signal processor plugin. The dynamics of extracellular glutamate within a given field were determined by calculating the average fluorescence intensity within a 10 x 10 pixel ROI (1 pixel at 4 x 4 binning = 15.6 μm) placed adjacent to the location of the stimulating electrode. Values for % $\Delta F/F$ were copied to GraphPad Prism (GraphPad Software, 7825 Fay Avenue, Suite 230, La Jolla, CA 92037 USA), where decay tau was calculated from the response peak (in the case of short bursts of activity) or the end of stimulation (in the case of longer high-frequency trains) using a single exponential nonlinear curve fit. To visually represent the time course of the response, I applied the "fire" heat map in ImageJ and used the "volume viewer" 3D plugin to display the response along the *z* (time) axis.

2.5 Pharmacology

All the drugs used for these experiments were from Tocris Bioscience (Bristol, United Kigdom). Drugs used in the study and their concentrations are as follows: dihydrokainic acid (DHK) (catalog # 0111), a competitive and selective GLT-1 blocker (EAAT-2; 300

μM); DL-threo-β-benzyloxyaspartic acid (DL-TBOA) (catalog #1223), a competitive and nonselective excitatory amino acid transporter blocker (10 and 100 μM); DNQX disodium salt (catalog # 231210), an AMPA/kainite receptor antagonist (20 μM); and D-AP-5(catalog#0106), a selective NMDA receptor antagonist (50 μM).

2.6 Experimental design and statistics

The statistical tests used included one-way ANOVA, one-way repeated-measures (RM) ANOVA, two-way ANOVA, two-way RM ANOVA, and linear regression. *Post hoc* tests included Tukey's, Bonferroni's, and Dunnett's tests. The statistical test used for each experiment is indicated in Results. *P* values of <0.05 were considered significant. Where indicated, *N* and *n* refer to the number of animals and slices used in each experiment, respectively.

Chapter 3 - Results

3.1 Characterization of glutamate dynamics in different brain regions

3.1.1 Extracellular glutamate dynamics in the hippocampus

The hippocampus has dense glutamatergic connections, many of which exhibit robust activity-dependent synaptic plasticity. The Schaffer collateral pathway, consisting of axons from the CA3 hippocampal sub-region that synapse onto CA1 dendrites in the stratum radiatum (Fig 2), is one of the most-commonly studied synaptic connections in the mammalian brain. I first examined activity-dependent regulation of extracellular glutamate dynamics within hippocampal circuitry by stimulating glutamate release at the CA3-CA1 synapse with a glass electrode placed in the Schaffer collateral pathway of iGluSnFR-injected mice (Fig 3*A*). iGluSnFR was expressed under the control of the neuron-specific synaptic promoter. Thus, the fluorescent signals quantified in the present study represent relative differences in the amount and time-course of synaptically-released glutamate sensed at the extracellular neuronal surface. The iGluSnFR reporter consists of a circularly-permuted GFP molecule fused to a glutamate binding domain. Upon glutamate binding, a conformational change increases the fluorescence intensity of GFP emission (Marvin et al., 2013). Therefore, the increase in fluorescent intensity can be used to quantify relative changes in the amount of glutamate released and the time to clear synaptically-released glutamate from the extracellular space following various patterns of presynaptic activity. Glutamate release and clearance rates were visualized in

real-time by high-speed widefield imaging (205 frames per second) of iGluSnFR transients in response to afferent stimulation of short bursts of activity (2, 5 and 10 pulses at 100 Hz) and longer trains of high frequency stimulation (HFS; 50 and 100 pulses at 100 Hz). The relative magnitude of glutamate release was measured by the peak iGluSnFR response (Fig 3*B*, 3*D*) and the clearance rate was measured by calculating the iGluSnFR decay tau immediately following the termination of the stimulation period (Fig 3*C*, *3E*), as described previously (Armbruster et al., 2016; Parsons et al., 2016). Not surprisingly, I found that increasing the number of pulses within the shorter bursts dramatically increased iGluSnFR peaks (Fig 3*D*, *N*=10, *n*=17, RM-ANOVA, $p<0.001$), with %ΔF/F values more than doubling as afferent stimulation increased from 2 to 10 pulses at 100 Hz. In contrast, glutamate clearance rates were comparatively stable over this stimulation range (Fig 3*E*) despite the clear increase in response size. When longer trains of HFS were employed, including 50 and 100 pulses at 100 Hz, glutamate clearance rates slowed over three-fold (Fig 3*E*, *N*=10, *n*=17, RM-ANOVA, $p<0.001$). Within a given stimulation paradigm, I did not find any significant correlation between the peak (i.e. largest amount of glutamate accumulation reached) and the decay tau (i.e. glutamate clearance rate) both for short bursts (Fig 4*A*) and longer trains of HFS (Fig 4*B*). These data demonstrate that glutamate clearance rates are more closely linked to the duration of presynaptic activity (i.e. short bursts vs. longer trains of HFS) than the amount of glutamate released.

To account for the number of axons recruited during electrical stimulation, I varied the stimulation intensity from 25 to 250 μA while holding the stimulation duration constant (5 pulses at 100 Hz; Fig. 5). Not surprisingly, increasing the stimulus intensity

resulted in larger iGluSnFR responses in the hippocampus (Fig. 5; N =4, n = 7). Stimulus intensity also had a small but consistent and significant effect on iGluSnFR decay tau; however, iGluSnFR response peaks were much more sensitive than decay to increasing stimulus strengths (Fig. 5*B–D*; N = 4, n = 7; two-way RM ANOVA; stimulus intensity, $p < 0.001$; peak vs decay, $p < 0.001$; interaction, $p < 0.001$). Therefore, recruiting more glutamate afferents with larger stimulus intensities dramatically enhances the size of the iGluSnFR response but has a relatively limited effect on decay kinetics. These data support the idea that clearance rates are more heavily influenced by the duration of afferent activity than the magnitude of release.

3.1.2 Extracellular glutamate dynamics in cortex

I repeated the above experiments in cortex as it has been widely studied brain area containing dense glutamatergic afferents. In the cortex (Fig. 6*A*), increasing the number of pulses dramatically increased the response size of iGluSnFR transients, in line with my expectations and my results obtained in the hippocampus (Fig. 6*B*, *D*; N =8, n = 11, RM ANOVA, $p < 0.001$). During short bursts of presynaptic activity, the mean decay tau increased from 2 to 10 pulses, although *post hoc* significance was only observed when longer trains of HFS were applied (Fig. 6*C*, *E*; N =8, n =11, RM ANOVA, $p < 0.001$). In response to short bursts of activity, there was no significant correlation between iGluSnFR %$\Delta F/F$ (peak) and decay measurements (Fig. 7*A*) as seen in the hippocampus; however, a strong association was observed following HFS protocols in the cortex (Fig. 7*B*), with larger responses taking longer to clear from the extracellular space.

To account for the number of axons recruited during electrical stimulation, I varied the stimulation intensity from 25 to 250 μA while holding the stimulation duration constant (5 pulses at 100 Hz; Fig. 8). Stimulus intensity also had a small but consistent and significant effect on iGluSnFR decay tau; however, iGluSnFR response peaks were much more sensitive than decay to increasing stimulus strengths, as seen in hippocampus (Fig. 8*B–D*; $N = 4$, $n = 9$; two-way RM ANOVA; stimulus intensity, $p < 0.001$; peak vs decay, $p < 0.001$; interaction, $p < 0.001$). Therefore, recruiting more glutamate afferents with larger stimulus intensities dramatically enhances the size of the iGluSnFR response but has a relatively limited effect on decay kinetics.

3.1.3 Extracellular glutamate dynamics in striatum

I repeated the above experiments in dorsal striatum (Fig. 9*A*). Again, the amount of evoked glutamate release was also highly sensitive to the number of pulses of afferent stimulation, as expected (Fig. 9 *B*, *D*; $N = 4$, $n = 8$, RM ANOVA, $p < 0.001$). The mean clearance rate increased as burst size increased from 2 to 10 pulses, but again, *post hoc* significance was only observed after longer trains of HFS (Fig. 9*C*, *E*; $N = 4$, $n = 8$, RM ANOVA, $p < 0.001$), similar to my observations in the cortex. Within a given stimulation paradigm, I observed no significant correlation between iGluSnFR $\%\Delta F/F$ and decay taus for short bursts (Fig. 10*A*) or longer trains of HFS (Fig. 10*B*), suggesting that like the hippocampus, striatal clearance rates are more dependent on the duration of presynaptic activity than the amount of glutamate release per se.

To account for the number of axons recruited during electrical stimulation, I varied the stimulation intensity from 25 to 250 μA while holding the stimulation duration constant

(5 pulses at 100 Hz; Fig. 11). Not surprisingly, increasing the stimulus intensity resulted in larger iGluSnFR responses in the striatum (Fig. 11; N =5, n = 11); stimulus intensity also had a small but consistent and significant effect on iGluSnFR decay tau; however, iGluSnFR response peaks were much more sensitive than decay to increasing stimulus strengths (Fig. 11*B–D*; N = 5, n = 11; two-way RM ANOVA; stimulus intensity, p < 0.001; peak vs decay, p <0.001; interaction, p<0.001). Therefore, recruiting more glutamate afferents with larger stimulus intensities dramatically enhances the size of the iGluSnFR response but has a relatively limited effect on decay kinetics. These data support the idea that clearance rates are more heavily influenced by the duration of afferent activity than the magnitude of release.

3.1.4 Extracellular glutamate dynamics in cerebellum

Lastly, I repeated the same experiment in the molecular layers of the cerebellum (12*A*). I was particularly interested in the cerebellum due to the transporter expression profile in this region, which is dominated by GLAST instead of GLT-1 (Zhou & Danbolt 2013). The amount of evoked glutamate release was also highly sensitive to the number of pulses of afferent stimulation, as expected (Fig. 12 *B*, *D*; N= 3, n = 9, RM ANOVA, p < 0.001). The mean clearance rate increased as burst size increased from 2 to 10 pulses, but again, *post hoc* significance was only observed after longer trains of HFS (Fig. 12*C*, *E*; N =3, n = 9, RM ANOVA, p < 0.001), similar to my observations in the cortex. Within a given stimulation paradigm, I observed no significant correlation between iGluSnFR %ΔF/F and decay taus for short bursts (Fig. 13*A*) or longer trains of HFS (Fig. 13*B*),

suggesting that like the hippocampus, cerebellar clearance rates are more dependent on the duration of presynaptic activity than the amount of glutamate release.

3.1.5 Comparison of extracellular glutamate dynamics between different brain regions

Although the general relationships between presynaptic activity and clearance rate appeared to be similar for the hippocampus, cortex, striatum and cerebellum, interesting regional differences were revealed when I directly compared glutamate clearance rates in the four regions in response to shorter bursts of presynaptic activity and longer trains of HFS (Fig. 14 *A*-C, 10 pulse data shown for representation), (Fig 15, *A, B)*. The data reveal that, both for shorter bursts (2, 5, 10 pulses at 100 Hz) and longer trains of HFS (50, 100 pulses at 100 Hz), the hippocampus exhibited the fastest mean clearance rates, while the striatum and particulalry the cerebellum showed the slowest mean clearance rates (Fig. 15 *A*; Two way RM- ANOVA brain region $p<0.001$, number of pulses $p<0.001$, interaction $p<0.001$; hippocampus $N=10$, $n=7$, cortex $N=8$, $n=11$, striatum $N=4$, $n=8$, cerebellum $N=3$, $n=9$).

Longer trains of HFS also revealed clear regional effects, with the hippocampus clearing glutamate the fastest and the cerebellum clearing glutamate the slowest (Fig. 15*B*, Two-Way RM-ANOVA, brain region $p<0.001$, number of pulses $p<0.001$, interaction $p=0.71$, hippocampus $N=10$, $n=7$, cortex $N=8$, $n=11$, striatum $N=4$, $n=8$, cerebellum $N=3$, $n=9$). In all, these data reveal clear regional and activity-dependent effects on glutamate clearance rates and highlight the need to study glutamate dynamics *in situ* and in response to synaptic activity.

As no mechanism exists to degrade glutamate from the extracellular space, the rate of glutamate clearance from its release site is dependent on both diffusion and transporter-mediated uptake. For example, the fast clearance rates observed in the hippocampus could be driven primarily by a fast diffusion rate or highly efficient transporter-mediated uptake. Here, I measured the relative rate of glutamate diffusion in hippocampus, cortex, striatum and cerebellum by stimulating glutamate release as before, but in the presence of a saturating concentration of TBOA (100 μM) (Diamond 2005), a non-selective glutamate transporter blocker. To prevent the potential excitotoxic effect of complete transporter blockade, I added both d-APV (50 μM; to block NMDAR) and DNQX (20 μM; to block AMPAR and kainite receptors) (Armbruster et al., 2016) to the bath. Glutamate receptor blockers alone have no effect on iGluSnFR profiles (Parsons et al., 2016). I saw significant regional differences among the four different brain regions for both the shorter bursts of activity (Figure 16*A*, hippocampus N=3, n=7, cortex N=4, n=6, striatum N=5, n=9, cerebellum N=3, n=9, RM Two Way ANOVA, number of pulses $p<0.001$, brain region $p<0.001$, interaction $p=0.017$) and longer trains of HFS (16*B*, hippocampus N=3, n=7, cortex N=4, n=6, striatum N=5, n=9, cerebellum N=3, n=9, RM Two Way ANOVA, number of pulses $p=0.1819$, brain region $p=0.2535$, interaction $p=0.4306$). Surprisingly, the cerebellum exhibited the fastest mean diffusion rates. This result is suggestive of a low capacity of transporter-mediated uptake in the cerebellum, and that the main contributor to glutamate clearance in this region is diffusion.

3.2. Role of glutamate transporters in glutamate clearance

3.2.1 Comparative role of Glutamate transporters in hippocampus

Prior work used a pharmacological approach to quantify the functional contribution of GLT-1 relative to other excitatory amino acid transporters by measuring STCs before and after bath application of a saturating concentration of DHK (300 μM) (Diamond and Jahr 2000). The authors calculated a decay ratio, simply defined as the STC decay tau after transporter inhibition divided by the decay tau before transporter inhibition, and determined that the GLT-1 contribution to total uptake was greater in the hippocampus compared with the cortex, but only in the first postnatal week (Hanson et al., 2015). Here, I applied the same approach to the iGluSnFR transients to calculate a DHK (300 μM) decay ratio, representing the relative contribution of GLT-1 transporters to overall clearance kinetics, and also calculated a TBOA (100 μM) decay ratio, representing the relative contribution of all transporters to overall clearance kinetics. Note that the latter is not possible with STC recordings, as the STC is completely inhibited by this concentration of TBOA. In the hippocampus (Fig. 17), blocking GLT-1 resulted in an approximate twofold increase in both the size of evoked iGluSnFR responses (Fig. 17*A*, *B*, *D*) as well as the time to clear, regardless of the amount of presynaptic activity (Fig. 17*A*, *C*, *E*). The observed twofold increase in clearance rates after GLT-1 inhibition is similar to the decay ratio observed previously for STCs (Hanson et al., 2015). Interestingly, when I applied TBOA (100 μM) to block all transporter-mediated uptake, decay ratios were approximately fivefold larger than the decay ratios observed after DHK

treatment (Fig. 17*E*; N =3, n =6; two-way RM ANOVA; treatment, $p < 0.001$; number of pulses, p =0.397; interaction, p =0.632), and TBOA had a slight but significant effect on increasing the size of the responses (peak) relative to DHK (Fig. 17*D*; N = 3, n = 6; two-way RM ANOVA; treatment, p =0.037; number of pulses, p =0.616; interaction, p = 0.698). For decay ratios, significant *post hoc* differences between the DHK and TBOA effects were observed for each stimulation paradigm tested (Fig. 17*E*; $p < 0.001$, Bonferroni's). The dramatic difference between the decay ratio obtained in TBOA compared with DHK indicates either that non-GLT-1 transporters can contribute substantially to uptake capacity when GLT-1 is dysfunctional or that GLT-1 plays much less of a role in glutamate uptake than previously thought. To address the latter possibility, I compared the effect of saturating DHK (300 μM) with a sub-saturating concentration of TBOA (10μM) previously shown to have the same effect as 300 μM DHK on STCs in the hippocampus (Diamond 2005). It was reasoned that if GLT-1 plays only a minor role in overall glutamate clearance, 10μM TBOA, a sub-saturating concentration (Diamond 2005), should have a greater effect than 300 μM DHK on iGluSnFR decay kinetics. I found that the decay ratio was not significantly different between 10 μM TBOA and 300 μM DHK (Fig. 18*B*; DHK, N=3, n=4; TBOA, N=4, n=6; two-way RM ANOVA, p>0.05), arguing against the interpretation that GLT-1 plays only a minor role in glutamate clearance. In all, my pharmacological data indicate that non-GLT-1 transporters contribute substantially to uptake capacity when GLT-1 is dysfunctional.

3.2.2 Comparative role of Glutamate transporters in cortex

I conducted the same experiments in cortex to determine the effect of DHK (300 μM) and TBOA (100 μM). I found a significant difference in peak response between DHK and TBOA (Figure 19*B, D*, *N*=5, *n*=7, RM Two Way ANOVA, treatment $p<0.001$, number of pulses $p=0.858$, interaction $p=0.999$) regardless of the amount of presynaptic activity. Despite the larger peak responses after DHK application, I again found that TBOA had a much more profound effect on glutamate clearance, with DHK only slowing clearance rates to a fraction of the effect observed after TBOA (Figure 19 *A, C, E*, *N*=5, *n*=7, RM Two Way ANOVA, treatment $p<0.001$, # of pulses $p=0.147$, interaction $p=0.451$).

I also compared the role of 10μM TBOA with 300μM DHK. I found that the decay ratio was not significantly different between 10 μM TBOA and 300 μM DHK (Fig. 20*B*; DHK, *N*=4, *n*=6; TBOA, *N*=3, *n*=4; two-way RM ANOVA, $p>0.05$). In all, my pharmacological data indicate that non-GLT-1 transporters contribute substantially to uptake capacity when GLT-1 is dysfunctional in the cortex.

3.2.3 Comparative role of Glutamate transporters in striatum

In the striatum, DHK and TBOA also had different effects on the amount of extracellular glutamate accumulation, with DHK facilitating extracellular glutamate accumulation and TBOA returning iGluSnFR peaks to control or lower than control values (Fig. 21*A*, *B*, *D*; N= 6, n =11, two-way RM ANOVA; treatment, $p < 0.001$; number of pulses, $p = 0.232$; interaction, $p = 0.040$). The significant interaction effect reflects the tendency for TBOA to suppress evoked glutamate release primarily at lower stimulus durations (Fig. 21*D*). Regardless of the peak response, I again found that DHK had a relatively small effect on clearance rates when compared with the effect of TBOA (Fig. 21 *A*, *C*, *E*; N =6, n =11, two-way RM ANOVA; treatment, p <0.001; number of pulses, $p = 0.105$; interaction, p =0.379), similar to the results obtained in the hippocampus and cortex. Together, these data suggest a complex effect of transporter dysfunction on activity-dependent glutamate release and that a saturating concentration of the GLT-1 blocker DHK only slows glutamate clearance to ~20 – 25% of that induced by nonselective transporter blockade with TBOA.

I also compared the role of 10 μM TBOA with 300 μM DHK in the striatum. I found that the decay ratio was not significantly different between 10 μM TBOA and 300 μM DHK (Fig. 22*B*; DHK, N=4, n=5; TBOA, N=3, n=6; two-way RM ANOVA, p>0.05). In all, my pharmacological data indicate that non-GLT-1 transporters contribute substantially to uptake capacity when GLT-1 is dysfunctional in striatum.

3.2.4 Comparative role of Glutamate transporters in cerebellum

In the cerebellum, DHK and TBOA had different effects on the total extracellular glutamate concentration which I measured as the peaks. I found that, unlike other brain regions, DHK (300 μM) did not increase the peak iGluSnFR response. TBOA increased extracellular glutamate accumulation but only for short bursts of activity with 2 pulses (Fig. 23*B, D*, N=3, n=6, RM Two Way ANOVA, treatment p=0.1205, number of pulses p<0.001, interaction p=0.0107). In terms of the decay ratios for DHK and TBOA, I did not find any significant differences between the decay ratio of DHK and decay ratio of TBOA in post hoc test except for the 2 pulses and 5 pulses stimulation. Two-way ANOVA revealed an overall significance of treatment (Fig. 23*C, E, N*=3, n=6, RM Two Way ANOVA, treatment p=0.0234, number of pulses p<0.001, interaction p=0.0006). Together these data show that GLT-1 plays only a minor role in glutamate clearance and that diffusion, particularly during long trains of activity, represents the main method of glutamate clearance in the cerebellum.

3.3. Effect of glutamate dynamic on ambient glutamate level

Glutamate transporters are responsible for the rapid removal of synaptically released glutamate from the extracellular space but also work to keep ambient levels of extracellular glutamate low in the absence of substantial neural activity. By maintaining the ambient concentration of extracellular glutamate low, glutamate transporters ensure a high signal-to-noise ratio during synaptic neurotransmission (Danbolt 2001). Therefore, I asked whether transporter inhibition affects ambient glutamate levels (as measured by raw, unstimulated iGluSnFR fluorescence; (Parsons et al., 2016)) differently in the hippocampus, cortex, striatum and cerebellum. Experiments were performed in the presence of D-APV (50 μM) and DNQX (20 μM). Interestingly, DHK (300 μM) had very little effect on basal iGluSnFR values in all four regions (Fig. 24), suggesting that any rise in ambient glutamate induced by GLT-1 inhibition is too low to be detected by iGluSnFR. However, when TBOA was applied, clear elevations in basal iGluSnFR fluorescence were detected in the cortex and striatum (Fig. 24*B*, *C*; ANOVA, $p<0.001$, and *post hoc* Dunnett's test of control vs TBOA, $p< 0.001$, for both the cortex and striatum), whereas the elevation observed in the hippocampus was modest in comparison (Fig. 24*A*; ANOVA, $p =0.027$, and *post hoc* Dunnett's test of control vs TBOA, $p >0.05$) and no elevation of basal iGluSnFR was observed in cerebellum (Fig. 24 *D,* ANOVA, $p>0.05$, *post hoc* Dunnett's test of control vs TBOA, $p>0.05$). Thus, similar to the clearance of evoked glutamate transients, non-GLT-1 transporters play a substantial role in the maintenance of low ambient levels of extracellular glutamate.

Chapter 4: Discussion

The time course of synaptically-released extracellular glutamate is shaped by transporter mediated uptake and the morphological properties of the extracellular space proximal to the release site (Danbolt 2001; Thomas, Tian, & Diamond 2011). It is important to understand how extracellular glutamate is regulated in the CNS, as excess extracellular glutamate can impair synaptic plasticity (Li et al., 2011) and promote excitotoxicity (Hardingham & Bading, 2010; Parsons & Raymond, 2014). It also has been implicated that deficits in GLT-1-mediated uptake and the subsequent pathological accumulation of extracellular glutamate can be associated with numerous conditions of the CNS including Alzheimer disease, Huntington disease and Amyotrophic Lateral Sclerosis (Behrens, Franz, Woodman, Lindenberg, & Landwehrmeyer, 2002; Howland et al., 2002; Huang et al., 2010; Liévens et al., 2001; Masliah, Alford, R, Mallory, & Hansen, 1996; Miller et al., 2008; Rothstein 1995; Scott, Gebhardt, Mitrovic, Vandenberg, & Dodd, 2011). Here, I used widefield iGluSnFR imaging (Armbruster et al., 2016; Marvin et al., 2013; Parsons et al., 2016; Pinky, Wilkie, Barnes, & Parsons, 2018) to characterize the real-time extracellular profiles of synaptically-released glutamate in various brain regions and in response to a wide range of synaptic stimulation.

4.1 Regional differences in glutamate clearance

By quantifying the decay kinetics of STCs in acute hippocampal slices, it was previously demonstrated that glutamate transporters are not overwhelmed by stimulus trains up to 10 pulses at 100 Hz (Diamond & Jahr 2000). I demonstrate a similar efficiency here in the hippocampus using iGluSnFR, but show that this efficiency is not observed in the cortex, striatum and cerebellum (Fig 15). In the cortex and striatum, increasing the number of pulses in the stimulus burst from 2 to 10 (100 Hz) increased the glutamate clearance time as shown by increasing decay tau suggesting that transporters in these regions become overwhelmed earlier than those in the hippocampus. Whereas in the cerebellum, the decay tau increased substantially more than that was observed in hippocampus, cortex and striatum. Furthermore, iGluSnFR decay rates were consistently faster in the hippocampus than in the cortex, striatum and cerebellum regardless of the amount of presynaptic activity (Fig 15), consistent with a recent observation of STCs at postnatal day 14, where cortical STC decay tau values were approximately two-fold slower than the same values in the hippocampus (Hanson et al., 2015). Interestingly, a recent study elegantly demonstrated using serial electron microscopy that the distance between astrocytes and the postsynaptic density is shorter in the hippocampus compared to the striatum (Chai et al., 2017), which may account for the enhanced efficiency of transporter mediated uptake in the hippocampus. In addition, prior integrative optical imaging and real-time iontophoresis experiments demonstrated that diffusion rates are faster in the hippocampus compared to the cortex (Hrabětová, 2005). It was also shown previously in cultures that the rate of glutamate uptake is slower in the cerebellum than

the cortex and striatum (Drejer, Larsson, & Schousboe, 1982) and I also observed the slowest glutamate clearance rates in the cerebellum in my experiments.

In the present study, relative diffusion rates of synaptically-released glutamate were quantified by monitoring iGluSnFR decay tau while blocking transporter-mediated uptake with 100 μM TBOA, and I found faster diffusion rates in the cerebellum compared to hippocampus, cortex and striatum, regardless of the amount of presynaptic activity, with a significant difference in cerebellum diffusion rate from cortex and striatum in lower pulses (Fig 16). It has been shown before that the glutamate transients received at cerebellar Bergmann glia is less than the glutamate transients at the extra-synaptic space and it remains elevated in the extra-synaptic space for many milliseconds (Bergles & Jahr 1997), which indicates the role of diffusion in cerebellum for glutamate clearance from a synaptic site. This suggests that the role of diffusion may be more important than transporter mediated uptake in the cerebellum. Among the non GLT-1 transporters, GLAST (in Bergmann glia) and EAAT4 (Purkinje cell membrane), the role of GLAST includes removing the neurotransmitter at early times just after glutamate is being released and EAAT4 removes glutamate at a later time point to prevent spillover to the neighbouring synapses (Takayasu et al., 2005). It has been illustrated that GLAST knockout had no effect on parallel fiber EPSC (Watase et al., 1998) and the role of glial glutamate transporters in cerebellum is to prevent the synaptic cross talk (Marcaggi, Billups, & Attwell, 2003), suggesting that diffusion mediates a substantial portion of glutamate clearance in the cerebellum, with uptake mechanisms acting largely as a backup to prevent synaptic crosstalk. It also has been demonstrated previously that, in

cerebellum, multi-vesicular release of glutamate can overwhelm nearby transporters (Foster, Kreitzer, & Regehr, 2002; Jacques I. Wadiche & Jahr, 2001), hence it is important for glutamate to diffuse from the synaptic cleft and then the cerebellar glutamate transporters could reduce the glutamate concentration from the extracellular space. Together, these data demonstrate clear regional- and activity-dependent differences in the rate of glutamate clearance with the efficient transporter mediated uptake in hippocampus and the very little role of transporter mediated uptake in cerebellum.

A recent study used both iGluSnFR and STC recordings to demonstrate that presynaptic activity influences glutamate clearance in the cortex (Armbruster et al., 2016). Here, I also observed a clear effect of presynaptic activity on the rate of glutamate clearance, with all tested regions showing a dramatic increase in the time required to clear extracellular glutamate following longer HFS trains of 50-100 pulses compared to shorter bursts of activity. As glutamate uptake is voltage dependent (Brew & Attwell, 1987), astrocyte depolarization during neural activity (Meeks & Mennerick, 2007) may account for the slow clearance rates observed following long stimulus trains. Furthermore, neural activity induces glial swelling and reduces the extracellular volume fraction, which can increase tortuosity and slow glutamate diffusion during long stimulus trains (Syková et al., 2008; Sykova, Vargova, Prokopova, & Simonova, 1999).

As mentioned earlier, I used both shorter (2,5,10 pulses) and longer (50, 100 pulses) trains of HFS. It was noticed that the profile of iGluSnFR during the long stimulation protocols shows a decay phase during the stimulation, which likely represents a combination of transmitter depletion and ongoing uptake/diffusion. This feature was noticed in hippocampus, cortex, striatum and cerebellum. My study focused on glutamate

clearance at the termination of neural activity. It is of the future interest to the lab to understand what processes are involved in shaping the iGluSnFR response during prolonged stimuli.

4.2 Effects of transporter inhibition on iGluSnFR responses

For the past two decades, it has been widely-reported that GLT-1 is responsible for the large majority of glutamate uptake in the brain, with percentages of 90% or higher often being cited in manuscript introductions and review articles. In my study, I found that while blocking GLT-1 with 300 μM DHK indeed prolonged the time course of evoked iGluSnFR transients, it produced only a fraction of the effect observed following 100 μM TBOA application. Interestingly, approximately half of the STC persists following a saturating concentration of DHK (Diamond & Jahr 2000; Thomas et al. 2011), which is likely to represent current through GLAST transporters which are also abundant on astrocyte membranes (Danbolt 2001). My data here strongly suggest that while GLT-1 may be the most abundant transporter in the brain, non-GLT-1 transporters can make large contributions to the rate glutamate clearance, particularly when GLT-1 is dysfunctional.

iGluSnFR also represents a powerful tool to study relative alterations in evoked presynaptic glutamate release. In the hippocampus, transporter inhibition by either DHK or TBOA increased the response peak over two-fold, indicating a facilitation of presynaptic release induced by transporter inhibition, in agreement with a previously reported increase in excitatory postsynaptic current (EPSC) amplitude following

transporter inhibition in the adult hippocampus (Diamond 2005). On the other hand, while DHK tended to increase response peaks in the cortex and striatum, response sizes were reduced in these regions following TBOA application, also in agreement with a prior observation of a TBOA-induced reduction of striatal EPSCs (Milnerwood et al., 2010). Transporter inhibition in the hypothalamus increases extracellular glutamate and reduces presynaptic release by activating presynaptic group III metabotropic glutamate receptors (Oliet, 2001). Here, TBOA had the greatest effect on ambient glutamate levels in the striatum and cortex, the two regions that exhibited a TBOA-induced depression of evoked glutamate release. Indeed, presynaptic mGluR activation has been shown to inhibit excitatory transmission at the corticostriatal synapse (Pisani, Calabresi, Centonze, & Bernardi, 1997) and in the deep layers of the cortex (Bandrowski, 2002). Thus, my results are consistent with electrophysiological observations of transporter inhibitor effects on EPSCs, and suggest that iGluSnFR can be used as a powerful tool to study glutamate transmission, both with respect to relative changes in release probability and extracellular clearance rates.

4.3 Quantifying glutamate clearance *in situ*: methodological considerations

STCs have been used to great effect to study glutamate dynamics *in situ*, and provides the greatest temporal resolution of the available methods, particularly when the filtering properties are mathematically eliminated from the STC kinetics (Diamond 2005). However, STCs are only able to sense glutamate at the surface of an individual astrocyte, are technically demanding and are extremely difficult to elicit in brain regions that have a low to moderate density of glutamate afferents. Widefield imaging of iGluSnFR

complements STCs in that they monitor extracellular glutamate sensed at the surface of a population of neurons (synapsin promoter) or astrocytes (GFAP promoter) and can be easily performed in multiple brain regions. However, iGluSnFR itself acts as a glutamate buffer and therefore exhibits slower absolute decay tau values compared to STCs under similar conditions. iGluSnFR affinity is in the μM range, and the values that I obtained from my present study as "%ΔF/F" match the values obtained by exogenous applications of μM concentrations of glutamate in the acute slice preparation (Parsons et al., 2016). This suggests that the slower iGluSnFR kinetics likely does not reflect the detection of very low glutamate concentrations which can not be detected by the STC Nonetheless, iGluSnFR's kinetics are sufficiently rapid to clearly resolve subtle relative differences in uptake capacity (Armbruster et al., 2016; Parsons et al., 2016).

4.4 Conclusion

The results of the present study demonstrate clear regional- and activity-dependent differences in the rate of glutamate clearance following synaptic activity and further highlight the importance of studying glutamate regulation *in situ*. The two major findings of the present study are as follows: 1) the hippocampus is more efficient at clearing extracellular glutamate compared to the cortex, striatum and cerebellum; and 2) GLT-1 inhibition by DHK only slowed clearance rates to a fraction of that induced by TBOA, suggesting non-GLT-1 transporters can make a substantial contribution to the glutamate clearance rate, particularly when GLT-1 is dysfunctional in hippocampus, striatum, cortex and cerebellum. The relative efficiency of glutamate clearance may play a role in dictating the type and magnitude of synaptic plasticity observed following long

trains of HFS. For example, the same HFS that produces clear long-term potentiation in the hippocampus results in presynaptically mediated long-term depression in the striatum. It is possible that the efficient uptake/clearance of glutamate in the hippocampus limits perisynaptic/extrasynaptic mGluR activity, which is required for HFS-induced striatal long-term depression (Sung, Choi, & Lovinger, 2001). Furthermore, slow clearance rates may play a role in regional vulnerability to excitotoxity. It is tempting to speculate that the slow clearance rates in the striatum can partially explain this region's vulnerability in Huntington disease, a devastating neurodegenerative disease in which glutamate toxicity and extrasynaptic NMDA receptor activation are major contributors to cell death (Milnerwood et al., 2010; Okamoto et al., 2009; Parsons & Raymond, 2014). Future research is required to fully understand the functional consequences of such dramatic regional differences in glutamate clearance, as the spatiotemporal dynamics of glutamate ultimately determines the location and types of glutamate receptors that are activated during neurotransmission.

Figures

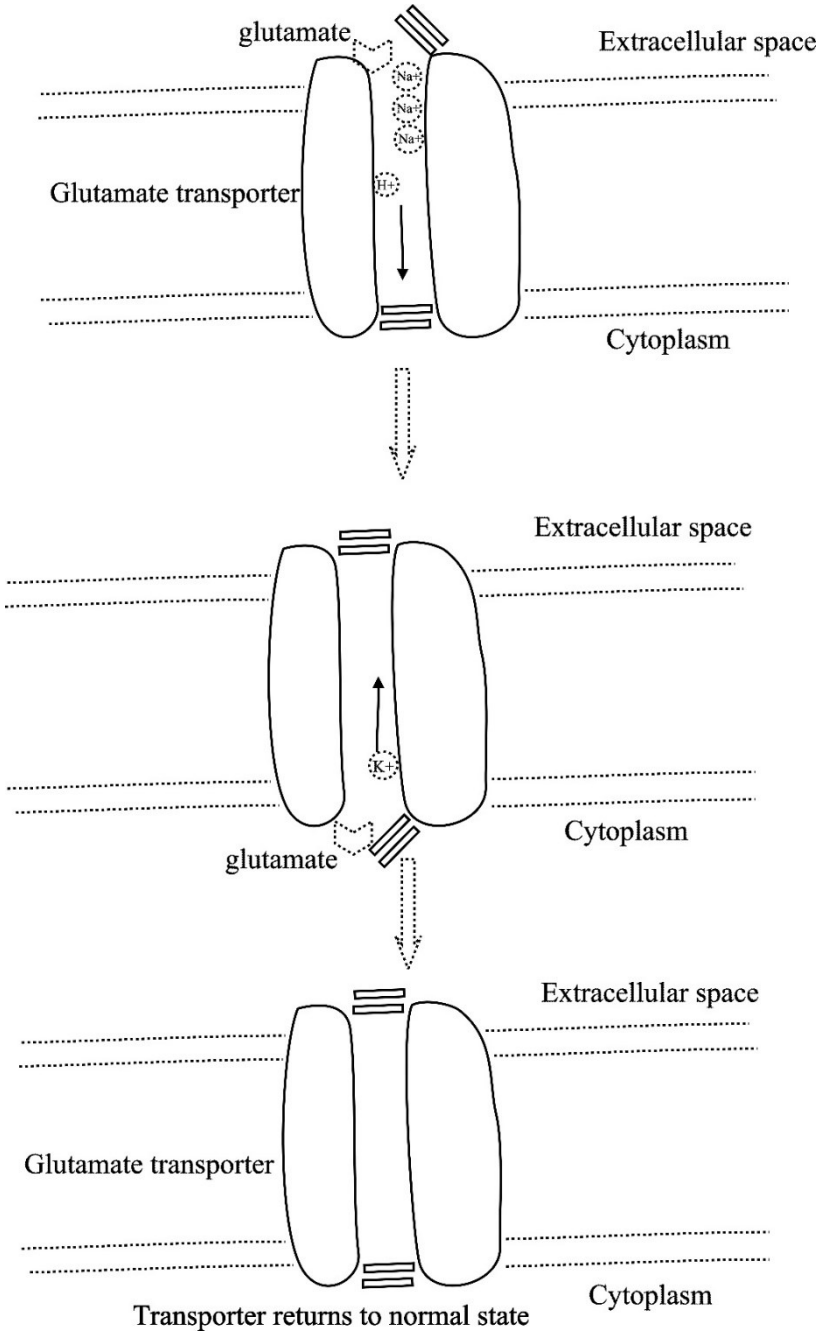

Figure 1: Adapted from (Tzingounis & Wadiche, 2007), showing the mechanism of action of glutamate transport across the cell membrane.

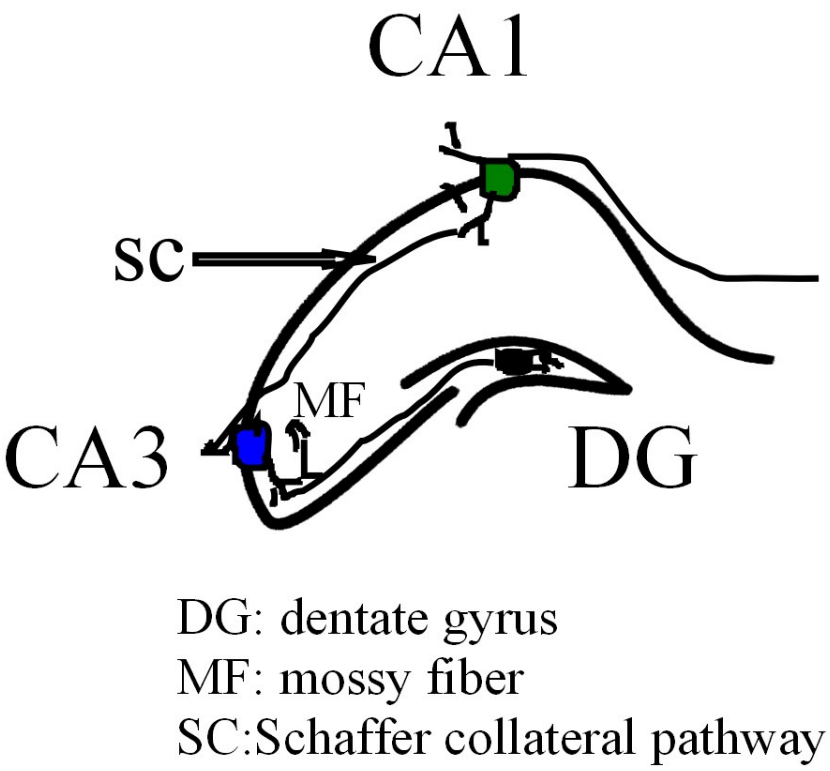

Figure 2: A diagram of hippocampal circuitry showing the Schaffer collateral pathway and mossy fiber pathway. The figure also shows the following areas in the hippocampus: Dentate gyrus (DG), CA3 and CA1.

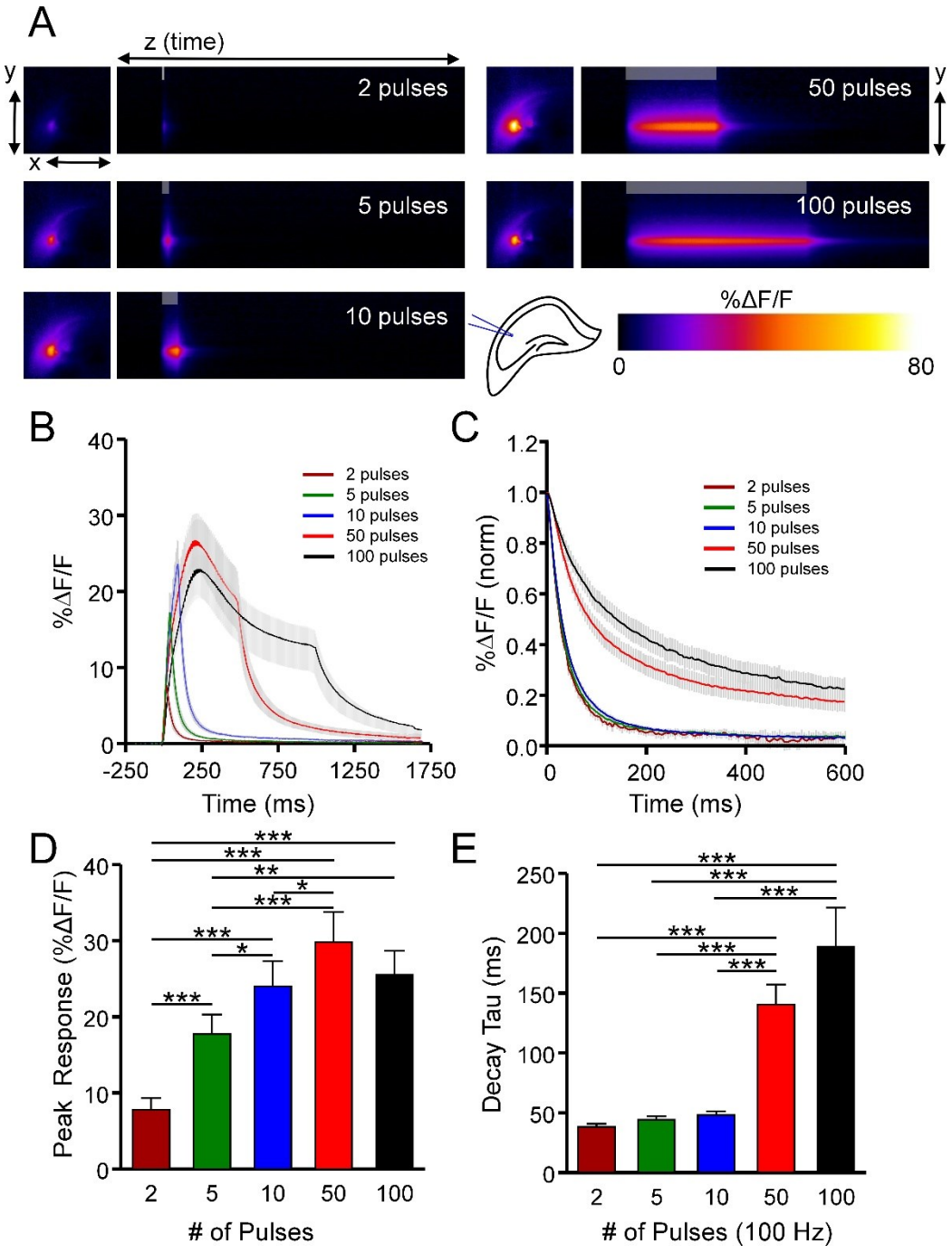
A
z (time)
y
x
2 pulses
5 pulses
10 pulses
50 pulses
100 pulses
%ΔF/F
0
80
B
%ΔF/F
Time (ms)
2 pulses
5 pulses
10 pulses
50 pulses
100 pulses
C
%ΔF/F (norm)
Time (ms)
D
Peak Response (%ΔF/F)
# of Pulses
E
Decay Tau (ms)
# of Pulses (100 Hz)

Figure 3: Characterization of extracellular glutamate dynamics in the hippocampus. ***A***, Representative heatmaps of iGluSnFR responses after afferent stimulation (100 Hz). Peak responses are shown in the *x–y* plane (image size, 2*2 mm), and the *y–z* (time) plots show the kinetics of the response at a defined *x*-coordinate adjacent to the site of stimulation (image represents 2 s). The gray shaded area within the images denotes the onset and duration of afferent stimulation. ***B***, Mean (±SEM) iGluSnFR response profiles to 2, 5, 10, 50, or 100 pulses of afferent stimulation at 100 Hz. ***C***, Mean responses (±SEM) From ***B*** that were normalized to the peak value at the end of the stimulation. ***D–E***, Grouped data showing mean (±SEM) iGluSnFR response peak (***D***) and decay tau (***E***). RM ANOVA with Tukey's *post hoc* results are indicated by *$p<0.05$ and ***$p<0.001$.

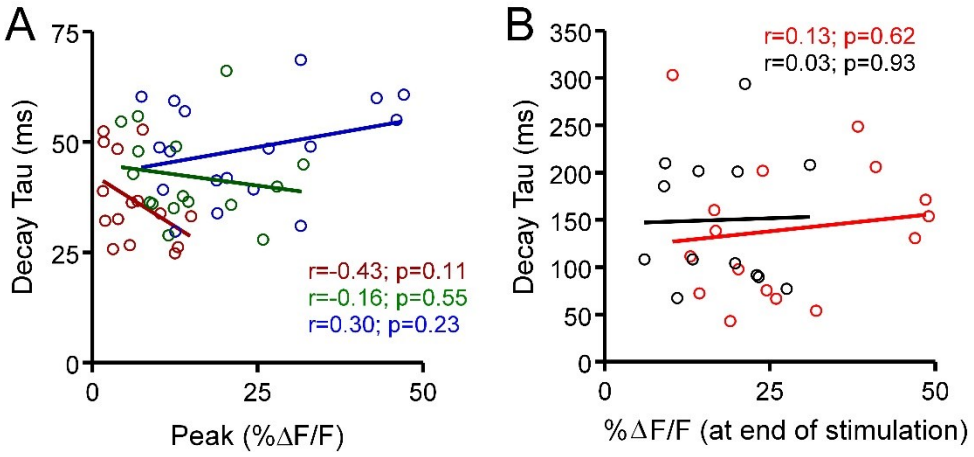

Figure 4: Relationship between iGluSnFR response peak and decay kinetics in the hippocampus. ***A-B***, Decay and Peak (%Δ*F*/*F*) correlation of the iGluSnFR responses with a short burst of activity (***A***) and longer trains of high frequency stimulation (***B***).

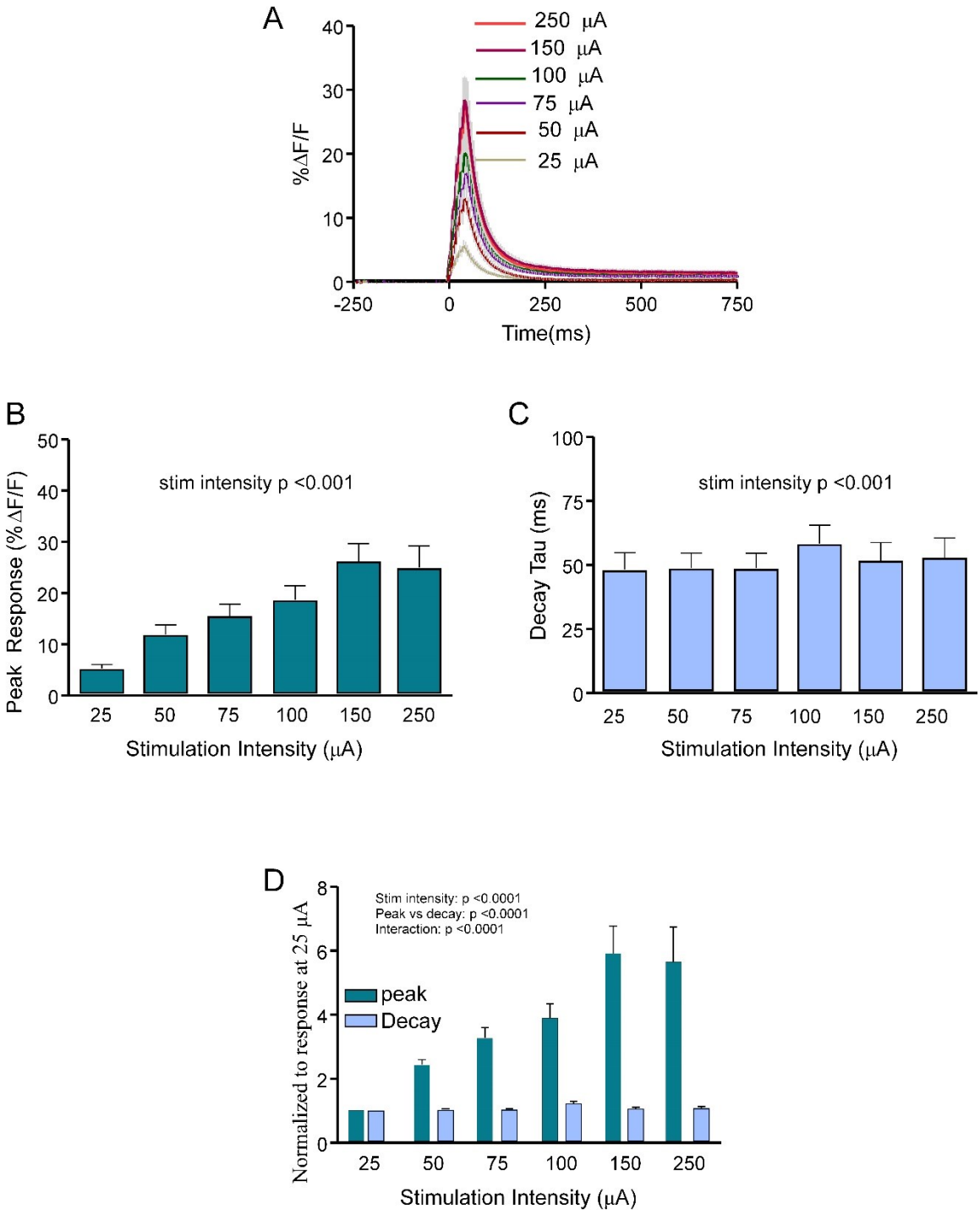
A
250 µA
150 µA
100 µA
75 µA
50 µA
25 µA
%ΔF/F
Time(ms)
B
stim intensity p <0.001
Peak Response (% ΔF/F)
Stimulation Intensity (µA)
C
stim intensity p <0.001
Decay Tau (ms)
Stimulation Intensity (µA)
D
Stim intensity: p <0.0001
Peak vs decay: p <0.0001
Interaction: p <0.0001
peak
Decay
Normalized to response at 25 µA
Stimulation Intensity (µA)

Figure 5: Effect of stimulus intensity on extracellular glutamate dynamics in the hippocampus. ***A***, Mean (±SEM) iGluSnFR response profiles in response to increasing the stimulus intensity (5 pulses, 100 Hz) from 25 to 250 μA. ***B-C****,* Grouped data showing mean (±SEM) iGluSnFR response peak (***B***) and decay tau (***C***) in response to increasing the stimulus intensity (5 pulses, 100 Hz) from 25 to 250 μA. RM ANOVA for ***(B, C)*** showed ***p<0.001.

D, Comparison of the effect of stimulus intensity on iGluSnFR peak and decay tau for the hippocampus, Data were normalized to the response at 25 μA. All *p* values were obtained by two-way RM ANOVA.

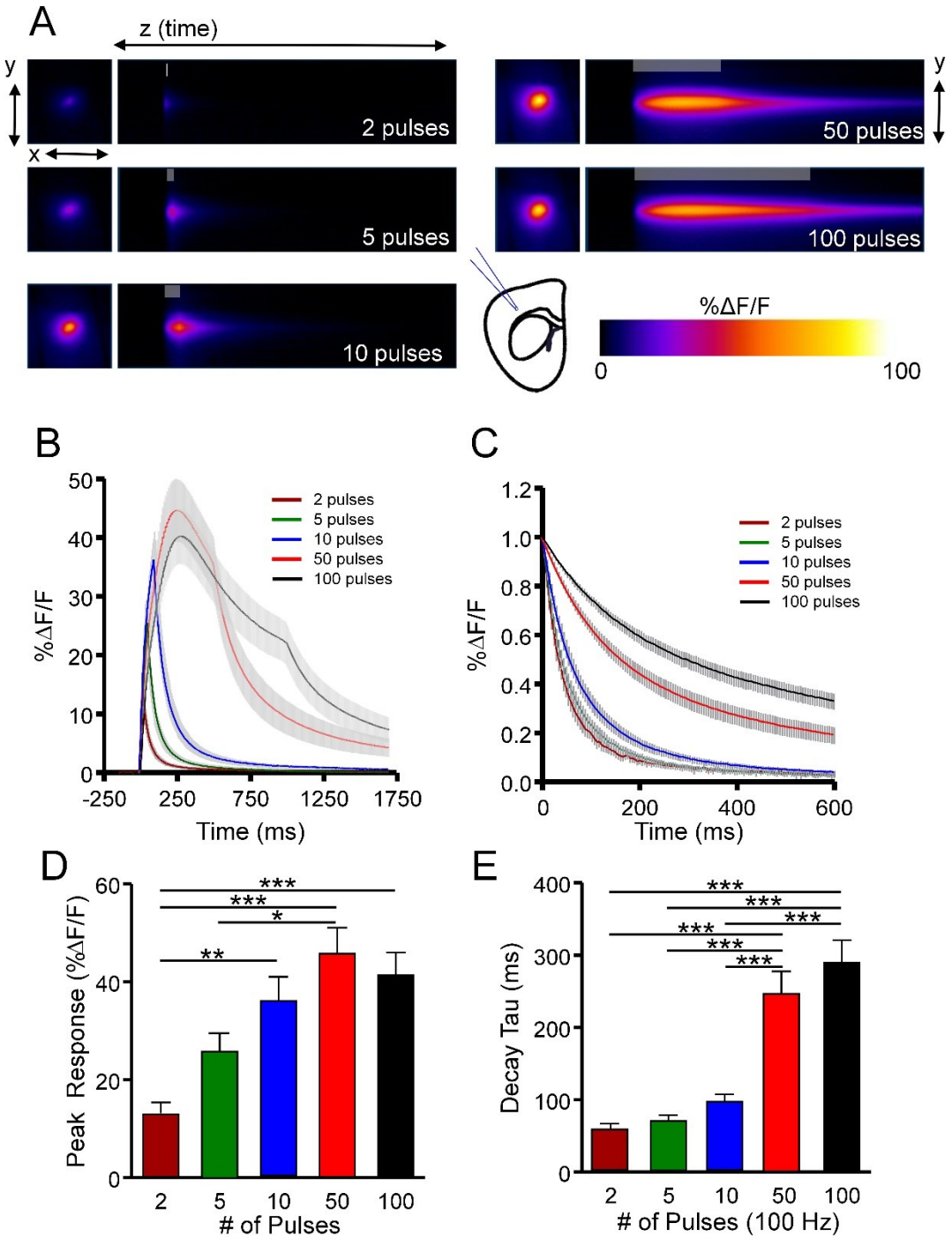
A
z (time)
y
x
2 pulses
5 pulses
10 pulses
50 pulses
100 pulses
%ΔF/F
0
100
B
%ΔF/F
Time (ms)
2 pulses
5 pulses
10 pulses
50 pulses
100 pulses
C
%ΔF/F
Time (ms)
D
Peak Response (%ΔF/F)
# of Pulses
E
Decay Tau (ms)
# of Pulses (100 Hz)

Figure 6: Characterization of extracellular glutamate dynamics in the cortex. ***A***, Representative heatmaps of iGluSnFR responses after afferent stimulation (100 Hz). Peak responses are shown in the *x*–*y* plane (image size, 2*2 mm), and the *y*–*z* (time) plots show the kinetics of the response at a defined *x*-coordinate adjacent to the site of stimulation (image represents 2 s). The gray shaded area within the images denotes the onset and duration of afferent stimulation. ***B***, Mean (±SEM) iGluSnFR response profiles to 2, 5, 10, 50, or 100 pulses of afferent stimulation at 100 Hz. ***C***, Mean responses (±SEM) From ***B*** that were normalized to the peak value at the end of the stimulation. ***D–E***, Grouped data showing mean (±SEM) iGluSnFR response peak (***D***) and decay tau (***E***). RM ANOVA with Tukey's *post hoc* results are indicated by *p<0.05,**p<0.01 and ***p<0.001.

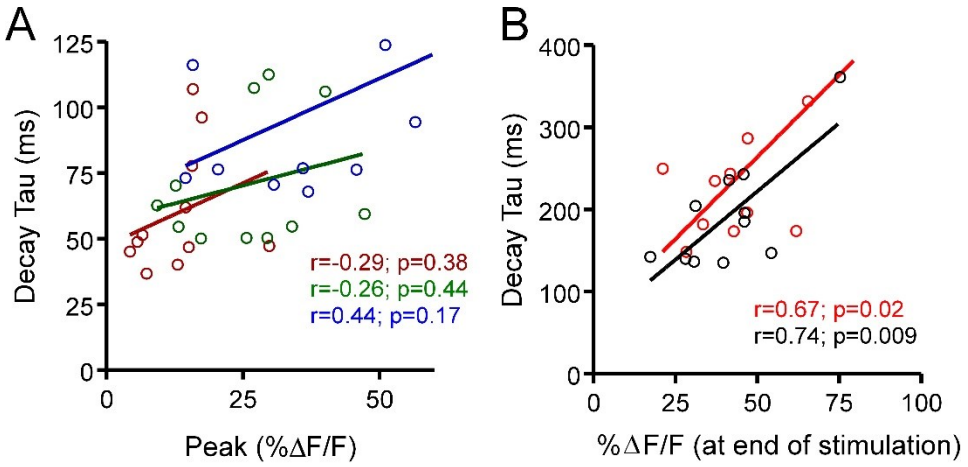

Figure 7: Relationship between iGluSnFR response peak and decay kinetics in the cortex. ***A-B***, Decay and Peak (%Δ*F*/*F*) correlation of the iGluSnFR responses with a short burst of activity (***A***) and longer trains of high frequency stimulation (***B***).

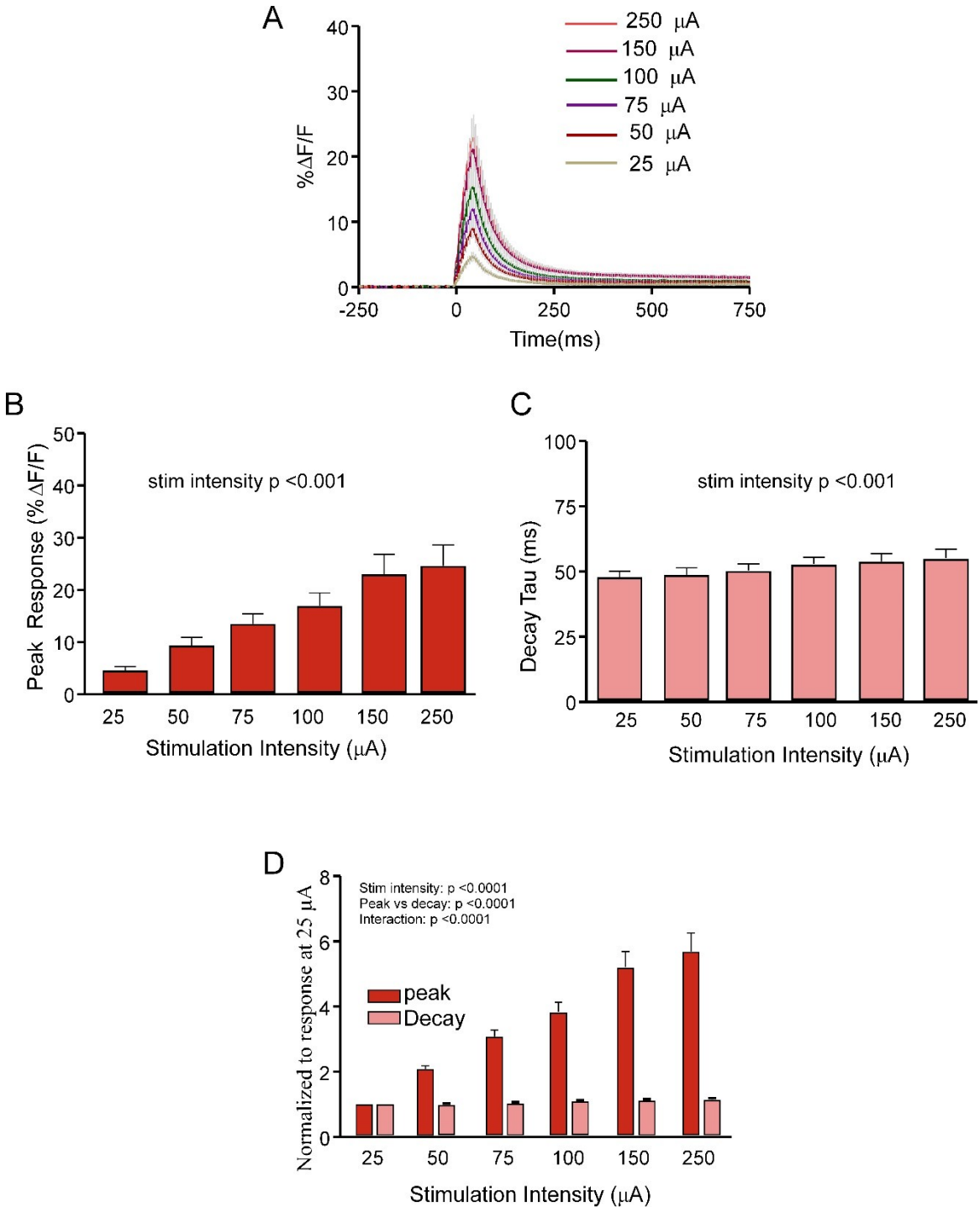
A
250 µA
150 µA
100 µA
75 µA
50 µA
25 µA
%ΔF/F
Time(ms)
B
stim intensity p <0.001
Peak Response (% ΔF/F)
Stimulation Intensity (µA)
C
stim intensity p <0.001
Decay Tau (ms)
Stimulation Intensity (µA)
D
Stim intensity: p <0.0001
Peak vs decay: p <0.0001
Interaction: p <0.0001
peak
Decay
Normalized to response at 25 µA
Stimulation Intensity (µA)

Figure 8: Effect of stimulus intensity on extracellular glutamate dynamics in the cortex. ***A***, Mean (±SEM) iGluSnFR response profiles in response to increasing the stimulus intensity (5 pulses, 100 Hz) from 25 to 250 µA. ***B-C****,* Grouped data showing mean (±SEM) iGluSnFR response peak (***B***) and decay tau (***C***) in response to increasing the stimulus intensity (5 pulses, 100 Hz) from 25 to 250 µA. RM ANOVA for ***(B, C)*** showed ***p<0.001.

D, Comparison of the effect of stimulus intensity on iGluSnFR peak and decay tau for the cortex, Data were normalized to the response at 25 µA. All *p* values were obtained by two-way RM ANOVA.

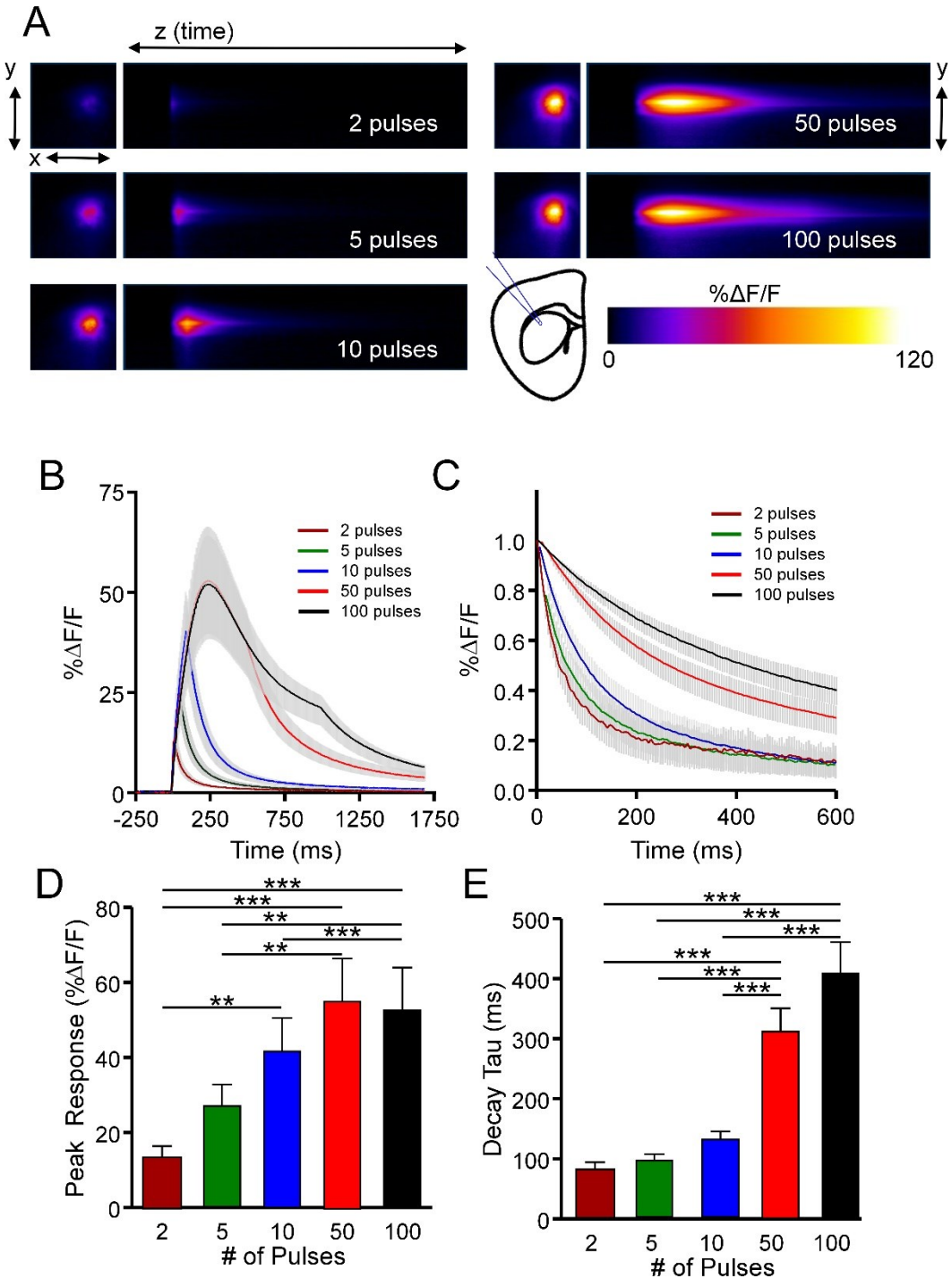
A
z (time)
y
x
2 pulses
5 pulses
10 pulses
50 pulses
100 pulses
%ΔF/F
0
120
B
%ΔF/F
Time (ms)
2 pulses
5 pulses
10 pulses
50 pulses
100 pulses
C
%ΔF/F
Time (ms)
D
Peak Response (%ΔF/F)
# of Pulses
E
Decay Tau (ms)
# of Pulses

Figure 9: Characterization of extracellular glutamate dynamics in the striatum. ***A***, Representative heatmaps of iGluSnFR responses after afferent stimulation (100 Hz). Peak responses are shown in the *x–y* plane (image size, 2*2 mm), and the *y–z* (time) plots show the kinetics of the response at a defined *x*-coordinate adjacent to the site of stimulation (image represents 2 s). The gray shaded area within the images denotes the onset and duration of afferent stimulation. ***B***, Mean (±SEM) iGluSnFR response profiles to 2, 5, 10, 50, or 100 pulses of afferent stimulation at 100 Hz. ***C***, Mean responses (±SEM) From ***B*** that were normalized to the peak value at the end of the stimulation. ***D–E***, Grouped data showing mean (±SEM) iGluSnFR response peak (***D***) and decay tau (***E***). RM ANOVA with Tukey's *post hoc* results are indicated by $^{**}p<0.01$ and $^{***}p<0.001$.

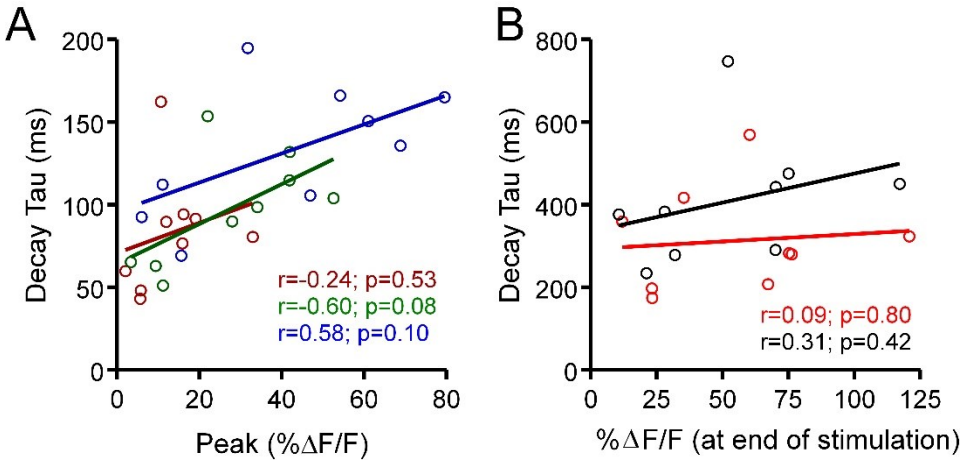

Figure 10: Relationship between iGluSnFR response peak and decay kinetics in the striatum. ***A-B***, Decay and Peak (%Δ*F*/*F*) correlation of the iGluSnFR responses with a short burst of activity (***A***) and longer trains of high frequency stimulation (***B***).

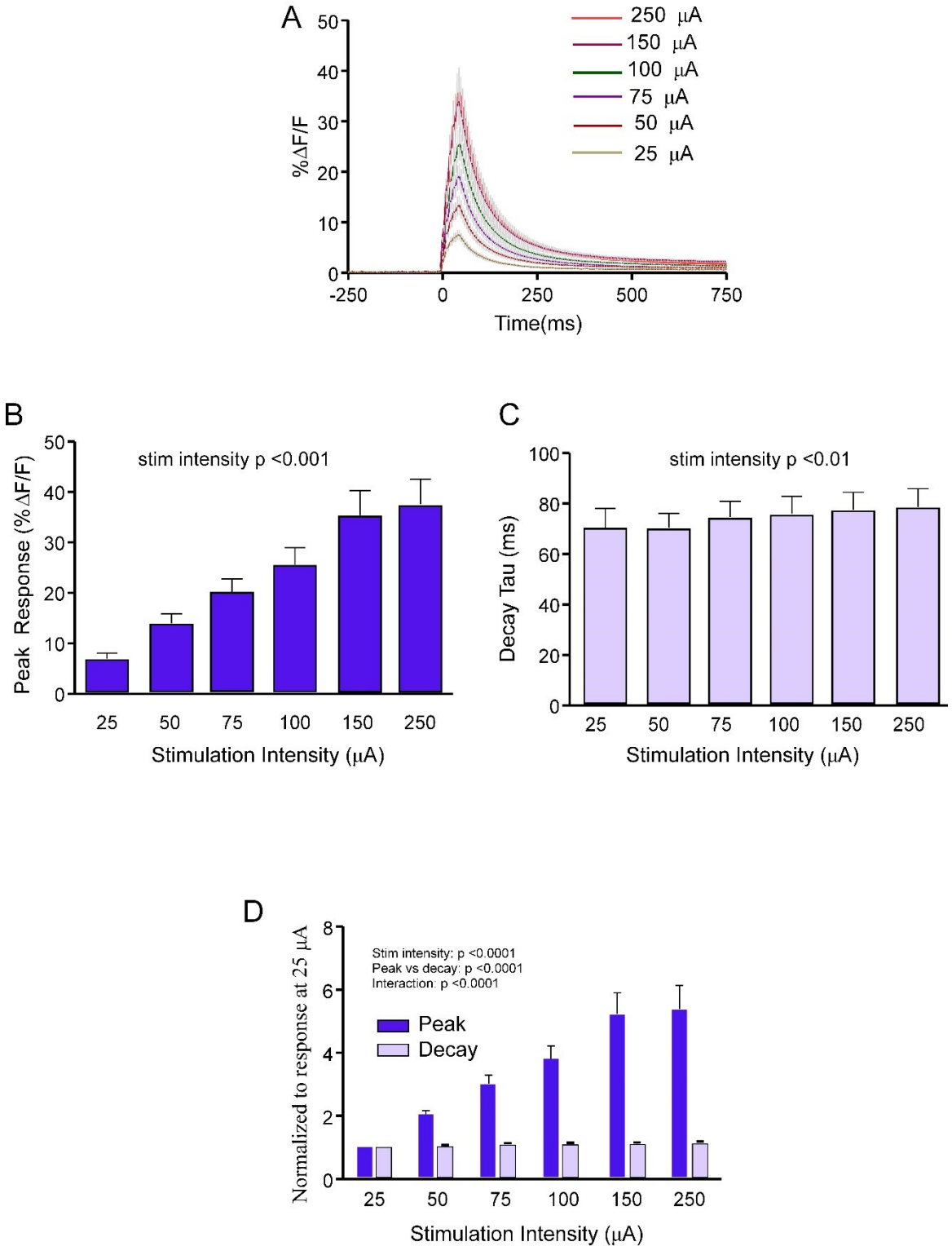
A
250 µA
150 µA
100 µA
75 µA
50 µA
25 µA
%ΔF/F
Time(ms)
B
stim intensity p <0.001
Peak Response (%ΔF/F)
Stimulation Intensity (µA)
C
stim intensity p <0.01
Decay Tau (ms)
Stimulation Intensity (µA)
D
Stim intensity: p <0.0001
Peak vs decay: p <0.0001
Interaction: p <0.0001
Peak
Decay
Normalized to response at 25 µA
Stimulation Intensity (µA)

Figure 11: Effect of stimulus intensity on extracellular glutamate dynamics in the striatum. ***A***, Mean (±SEM) iGluSnFR response profiles in response to increasing the stimulus intensity (5 pulses, 100 Hz) from 25 to 250 μA. ***B-C****,* Grouped data showing mean (±SEM) iGluSnFR response peak (***B***) and decay tau (***C***) in response to increasing the stimulus intensity (5 pulses, 100 Hz) from 25 to 250 μA. RM ANOVA for ***(B, C)*** showed ***p<0.001 ***(B)*** and **p<0.01 ***(C)***

D, Comparison of the effect of stimulus intensity on iGluSnFR peak and decay tau for the striatum, Data were normalized to the response at 25 μA. All *p* values were obtained by two-way RM ANOVA.

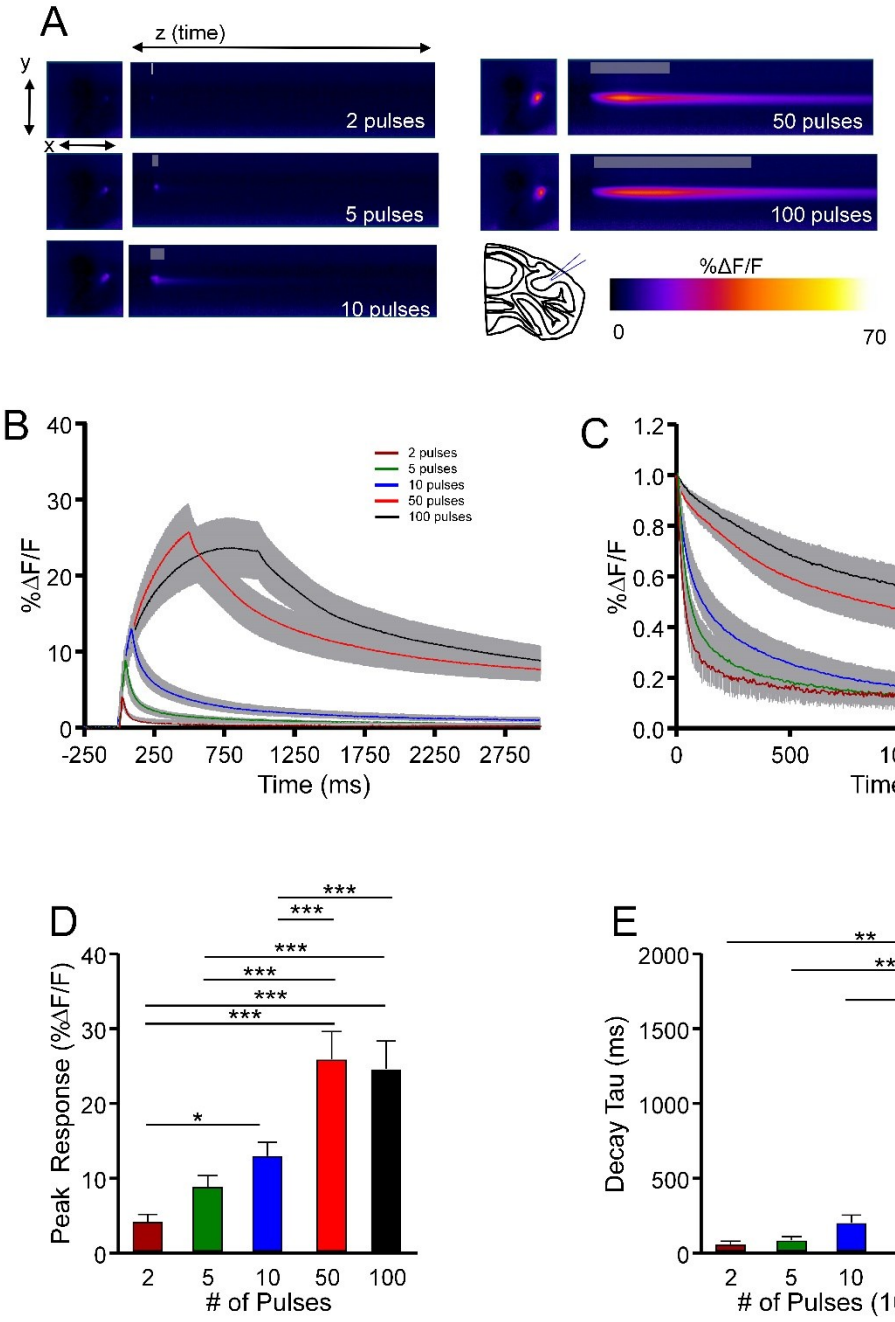
A
z (time)
y
x
2 pulses
5 pulses
10 pulses
50 pulses
100 pulses
%ΔF/F
0
70
B
%ΔF/F
Time (ms)
2 pulses
5 pulses
10 pulses
50 pulses
100 pulses
C
%ΔF/F
Time (ms)
2 pulses
5 pulses
10 pulses
50 pulses
100 pulses
D
Peak Response (%ΔF/F)
# of Pulses
E
Decay Tau (ms)
# of Pulses (100 Hz)

Figure 12: Characterization of extracellular glutamate dynamics in the cerebellum. ***A***, Representative heatmaps of iGluSnFR responses after afferent stimulation (100 Hz). Peak responses are shown in the *x–y* plane (image size, 2*2 mm), and the *y–z* (time) plots show the kinetics of the response at a defined *x*-coordinate adjacent to the site of stimulation (image represents 2 s). The gray shaded area within the images denotes the onset and duration of afferent stimulation. ***B***, Mean (±SEM) iGluSnFR response profiles to 2, 5, 10, 50, or 100 pulses of afferent stimulation at 100 Hz. ***C***, Mean responses (±SEM) From ***B*** that were normalized to the peak value at the end of the stimulation. ***D–E***, Grouped data showing mean (±SEM) iGluSnFR response peak (***D***) and decay tau (***E***). RM ANOVA with Tukey's *post hoc* results are indicated by *$p<0.05$, **$p<0.01$ and ***$p<0.001$.

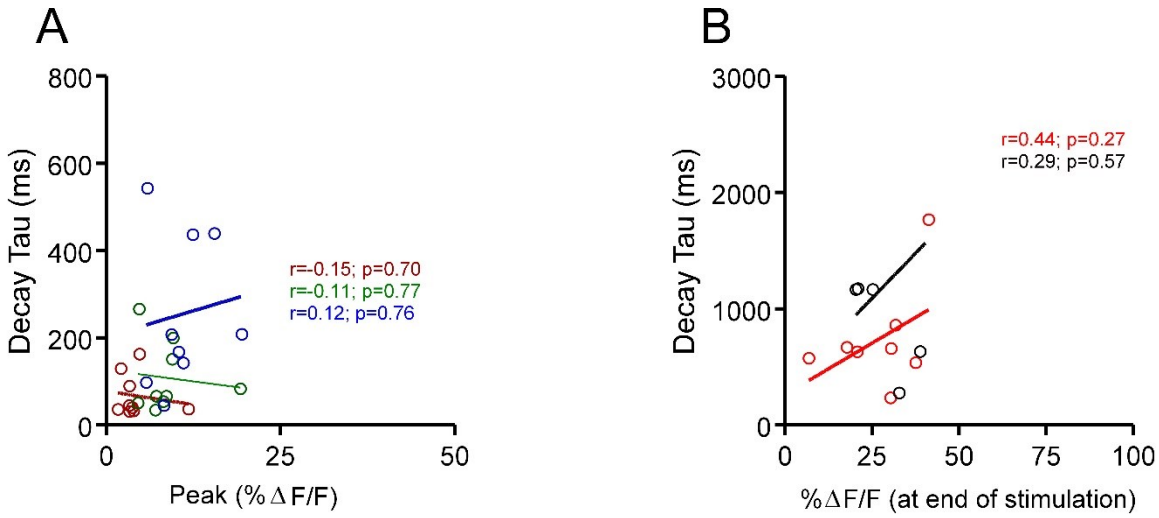

Figure 13: Relationship between iGluSnFR response peak and decay kinetics in the cerebellum. ***A-B,*** Decay and Peak (%Δ*F*/*F*) correlation of the iGluSnFR responses with a short burst of activity (***A***) and longer trains of high frequency stimulation (***B***).

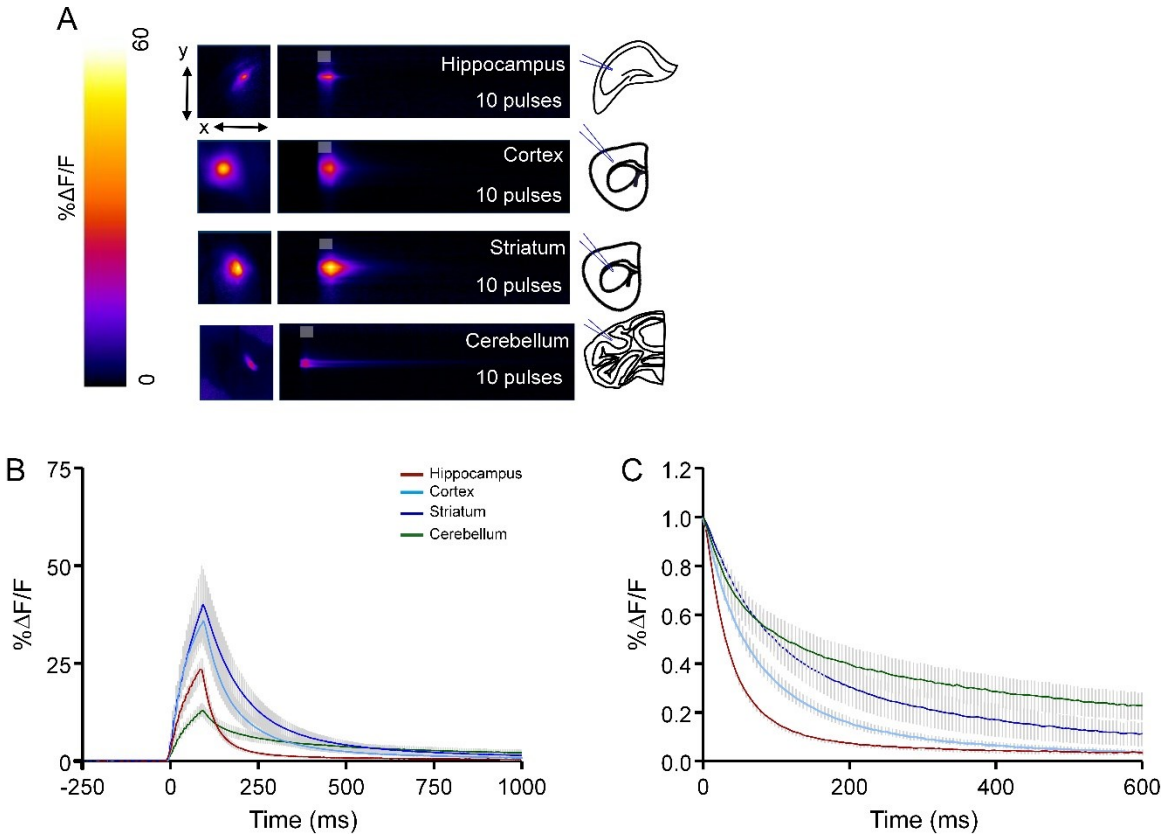

Figure 14: ***(A)*** Regional differences in glutamate clearance capacity. ***A***, Representative heatmaps of iGluSnFR responses in the hippocampus, cortex, striatum and cerebellum after afferent stimulation (10 pulses at 100 Hz). Peak responses are shown in the *x–y* plane (image size, 2*2 mm), and the *y–z* (time) plots show the kinetics of the response at a defined *x*-coordinate adjacent to the site of stimulation (image represents 2 s). The gray shaded area within the images denotes the onset and duration of afferent stimulation. ***B***, Mean (±SEM) iGluSnFR responses in the hippocampus, cortex, striatum and cerebellum to 10 pulses at 100 Hz. ***C***, Mean responses (±SEM) from ***B*** that were normalized to the peak value at the end of the stimulation.

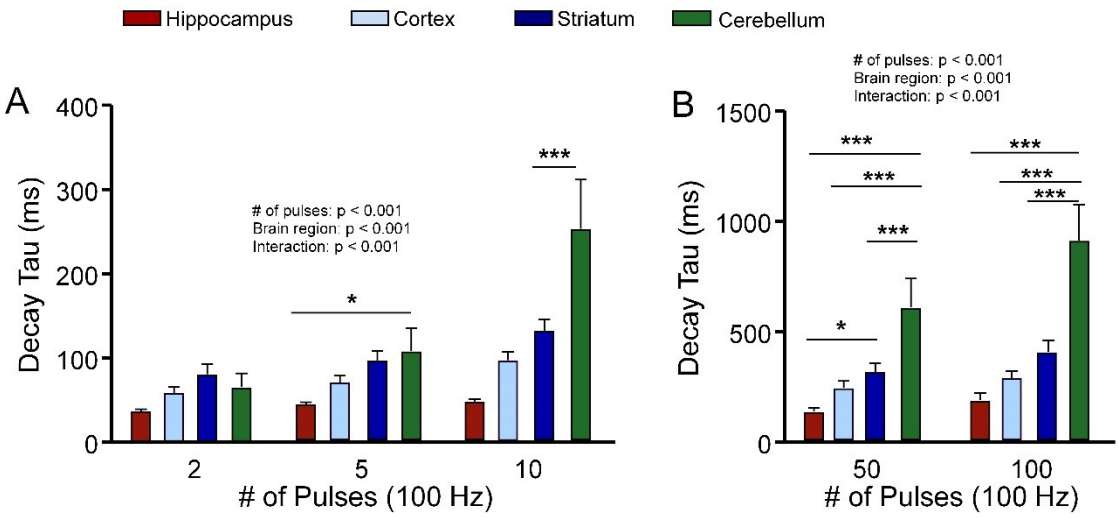

Figure 15: Regional differences in glutamate clearance capacity showed by iGluSnFr decay kinetics in hippocampus, cortex, striatum and cerebellum. ***(A, B)***, Regional comparison of mean (±SEM) iGluSnFR decay tau values showing fastest glutamate clearance rates in the hippocampus, for both shorter bursts of activity (***A***) and longer trains of high-frequency stimulation (***B***). Two way ANOVA with Bonferroni post hoc test, *p<0.05 and ***p<0.001.

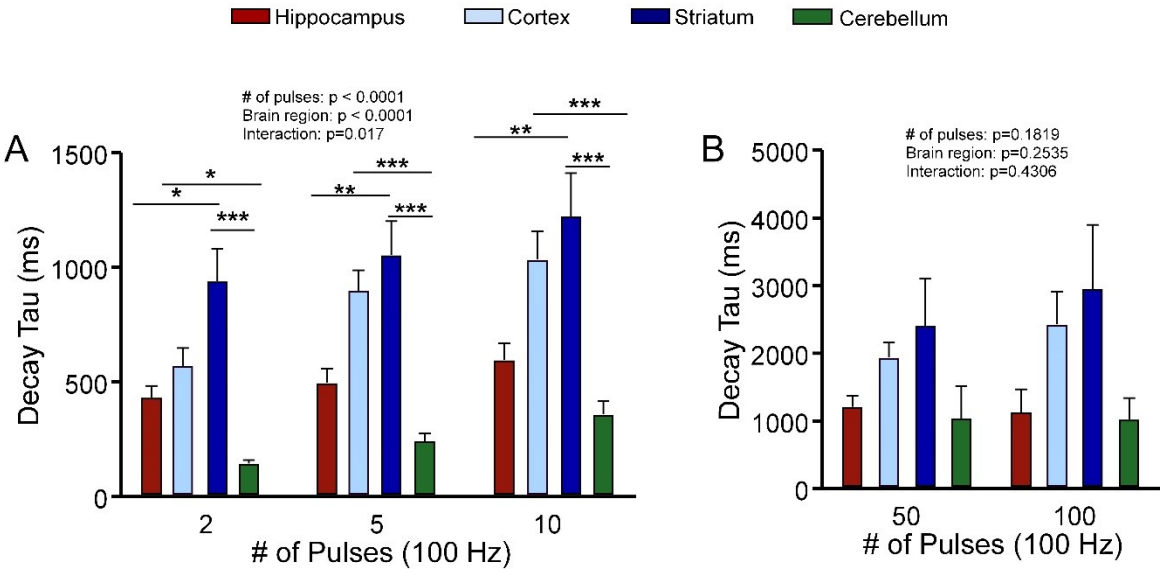

Figure 16: Regional differences in glutamate clearance capacity showed by iGluSnFr decay kinetics in hippocampus, cortex, striatum and cerebellum during glutamate transporter blockade with TBOA (100 µM) to quantify relative glutamate diffusion rates. ***(A, B)***, Regional comparison of mean (±SEM) iGluSnFR decay tau values showing fastest glutamate clearance rates in the cerebellum after TBOA (100 µM), for both shorter bursts of

activity (***A***) and longer trains of high-frequency stimulation (***B***). Two way ANOVA with Bonferroni post hoc test, *p<0.05, **p<0.01 and ***p<0.001

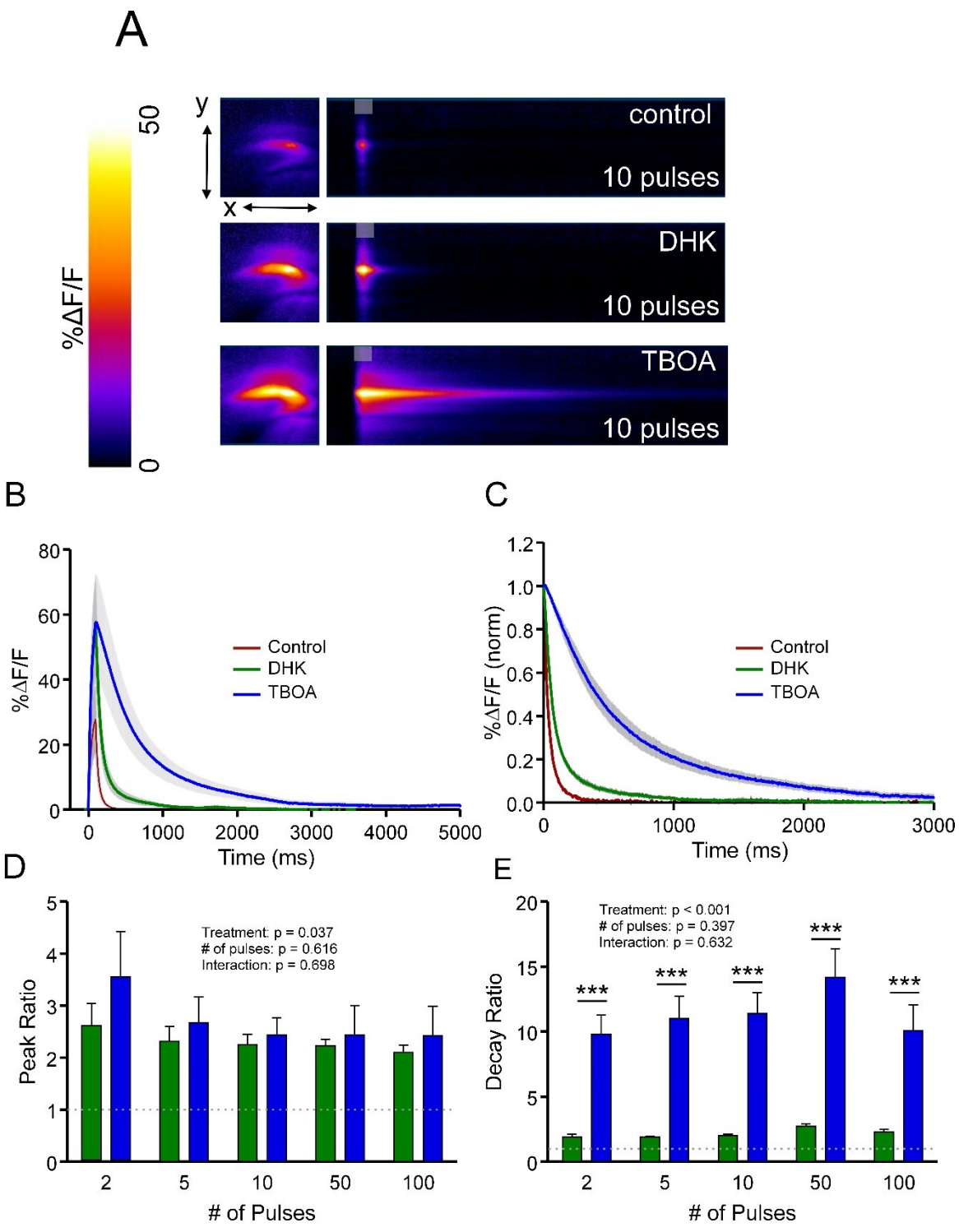
A
50
0
%ΔF/F
y
x
control
10 pulses
DHK
10 pulses
TBOA
10 pulses
B
%ΔF/F
Time (ms)
Control
DHK
TBOA
C
%ΔF/F (norm)
Time (ms)
Control
DHK
TBOA
D
Peak Ratio
Treatment: p = 0.037
# of pulses: p = 0.616
Interaction: p = 0.698
# of Pulses
E
Decay Ratio
Treatment: p < 0.001
# of pulses: p = 0.397
Interaction: p = 0.632
***
# of Pulses

Figure 17: Comparison of the effects of selective GLT-1 inhibition and nonselective transporter inhibition on glutamate dynamics in the hippocampus. ***A***, Representative heatmaps of hippocampal iGluSnFR responses after afferent stimulation (10 pulses at 100 Hz) in control conditions and after GLT-1 blockade with DHK (300 μM) and nonselective glutamate transporter blockade with TBOA (100 μM). Peak responses are shown in the *x–y* plane (image size, 2*2 mm), and the *y–z* (time) plots show the kinetics of the response at a defined *x*-coordinate adjacent to the site of stimulation (image represents 2 s). The gray shaded area within the images denotes the onset and duration of afferent stimulation. ***B***, Mean (±SEM) iGluSnFR response profiles to 10 pulses of afferent stimulation at 100 Hz in control, DHK, and TBOA conditions. ***C***, Mean responses (±SEM) from ***B*** that were normalized to the peak value at the end of the stimulation. ***D–E***, Grouped data showing mean (±SEM) DHK and TBOA peak ratios (***D***) and decay ratios (***E***) over a variety of stimulation paradigms. Peak and decay ratios indicate the fold effect of drug treatment over control levels. Two-way RM ANOVA with Bonferroni's *post hoc* results are indicated by ***p <0.001.

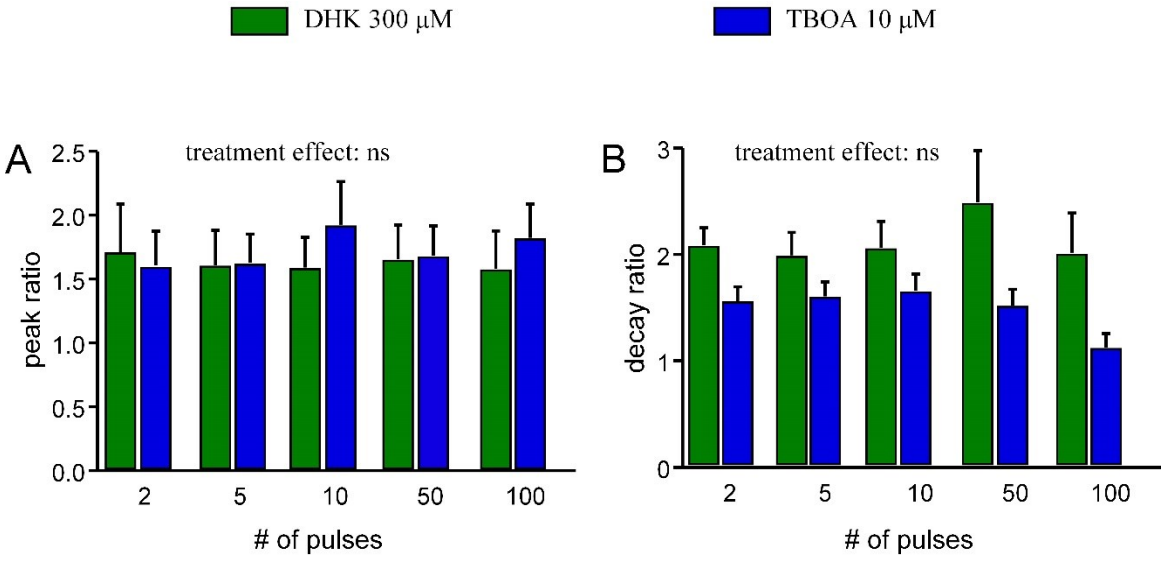

Figure 18: Comparison of the effects of selective GLT-1 inhibition and nonselective transporter inhibition on glutamate dynamics in the hippocampus. Grouped data showing mean (± SEM) DHK and TBOA peak ratios ***(A)*** and decay ratios ***(B)*** in hippocampus over a variety of stimulation paradigms while applying 300 μM DHK and 10 μM TBOA. Two way ANOVA showed non-significant treatment effect between 300 μM DHK and 10 μM TBOA.

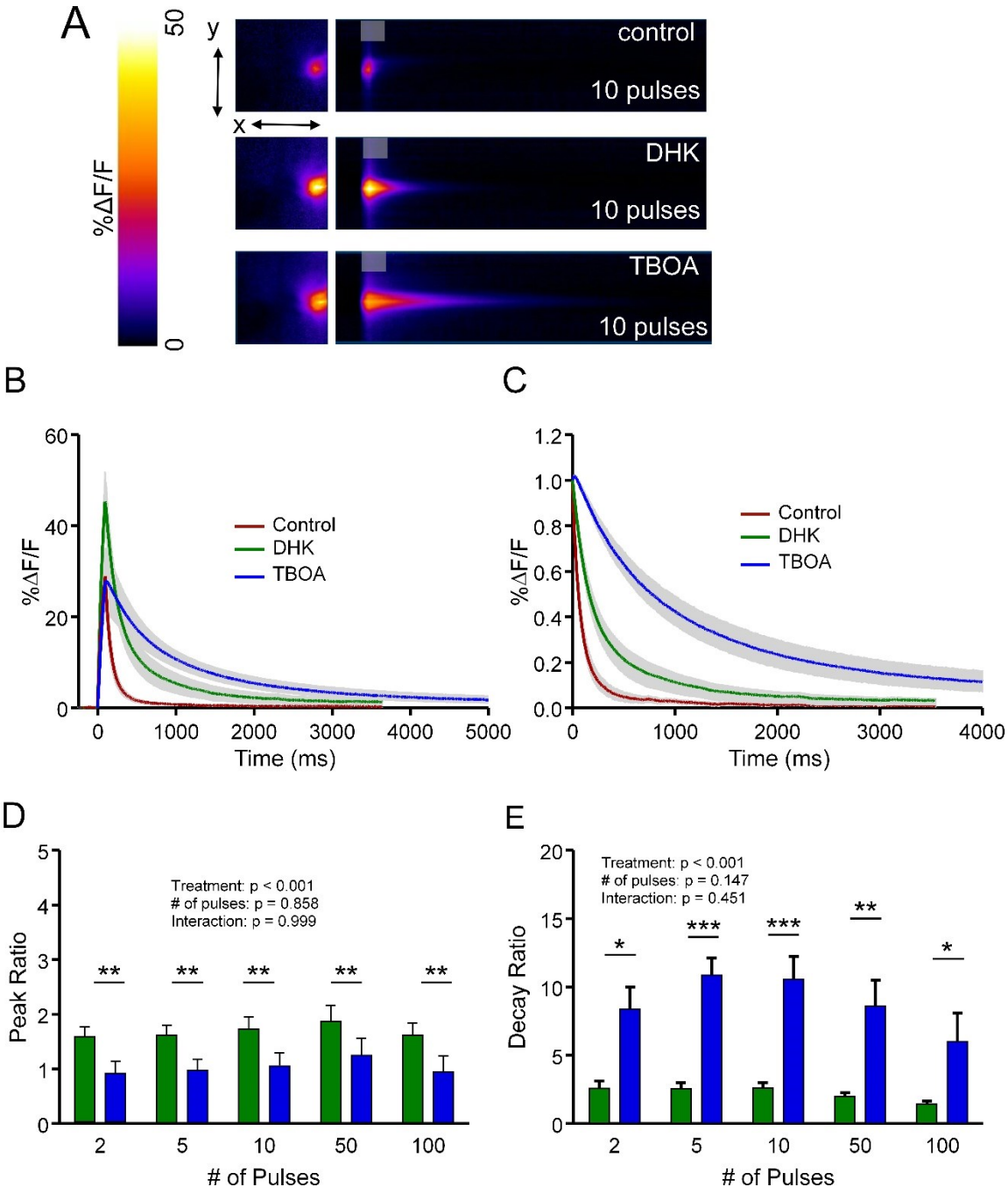
A
50
0
%ΔF/F
y
x
control
10 pulses
DHK
10 pulses
TBOA
10 pulses
B
%ΔF/F
Control
DHK
TBOA
Time (ms)
C
%ΔF/F
Control
DHK
TBOA
Time (ms)
D
Peak Ratio
Treatment: p < 0.001
# of pulses: p = 0.858
Interaction: p = 0.999
# of Pulses
E
Decay Ratio
Treatment: p < 0.001
# of pulses: p = 0.147
Interaction: p = 0.451
# of Pulses

Figure 19: Comparison of the effects of selective GLT-1 inhibition and nonselective transporter inhibition on glutamate dynamics in the cortex. ***A***, Representative heatmaps of cortex iGluSnFR responses after afferent stimulation (10 pulses at 100 Hz) in control conditions and after GLT-1 blockade with DHK (300 μM) and nonselective glutamate transporter blockade with TBOA (100 μM). Peak responses are shown in the *x–y* plane (image size, 2*2 mm), and the *y–z* (time) plots show the kinetics of the response at a defined *x*-coordinate adjacent to the site of stimulation (image represents 2 s). The gray shaded area within the images denotes the onset and duration of afferent stimulation. ***B***, Mean (±SEM) iGluSnFR response profiles to 10 pulses of afferent stimulation at 100 Hz in control, DHK, and TBOA conditions. ***C***, Mean responses (±SEM) from ***B*** that were normalized to the peak value at the end of the stimulation. ***D–E***, Grouped data showing mean (±SEM) DHK and TBOA peak ratios (***D***) and decay ratios (***E***) over a variety of stimulation paradigms. Peak and decay ratios indicate the fold effect of drug treatment over control levels. Two-way RM ANOVA with Bonferroni's *post hoc* results are indicated by *p <0.05, **p <0.01 and ***p <0.001.

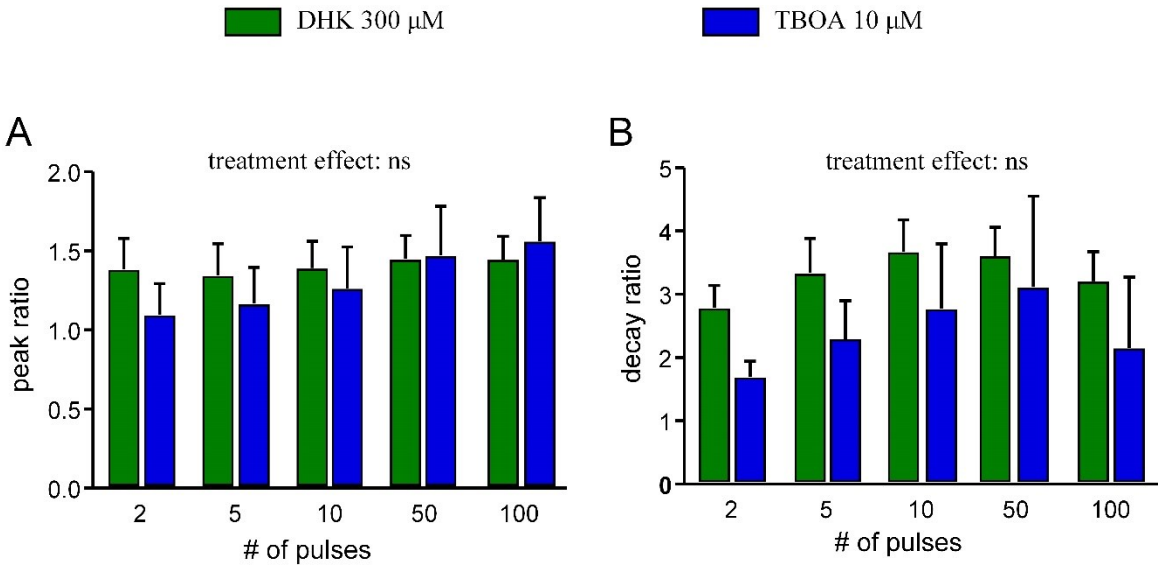

Figure 20: Comparison of the effects of selective GLT-1 inhibition and nonselective transporter inhibition on glutamate dynamics in the cortex. Grouped data showing mean (± SEM) DHK and TBOA peak ratios ***(A)*** and decay ratios ***(B)*** in cortex over a variety of stimulation paradigms while applying 300 µM DHK and 10 µM TBOA. Two way ANOVA showed non-significant treatment effect between 300 µM DHK and 10 µM TBOA.

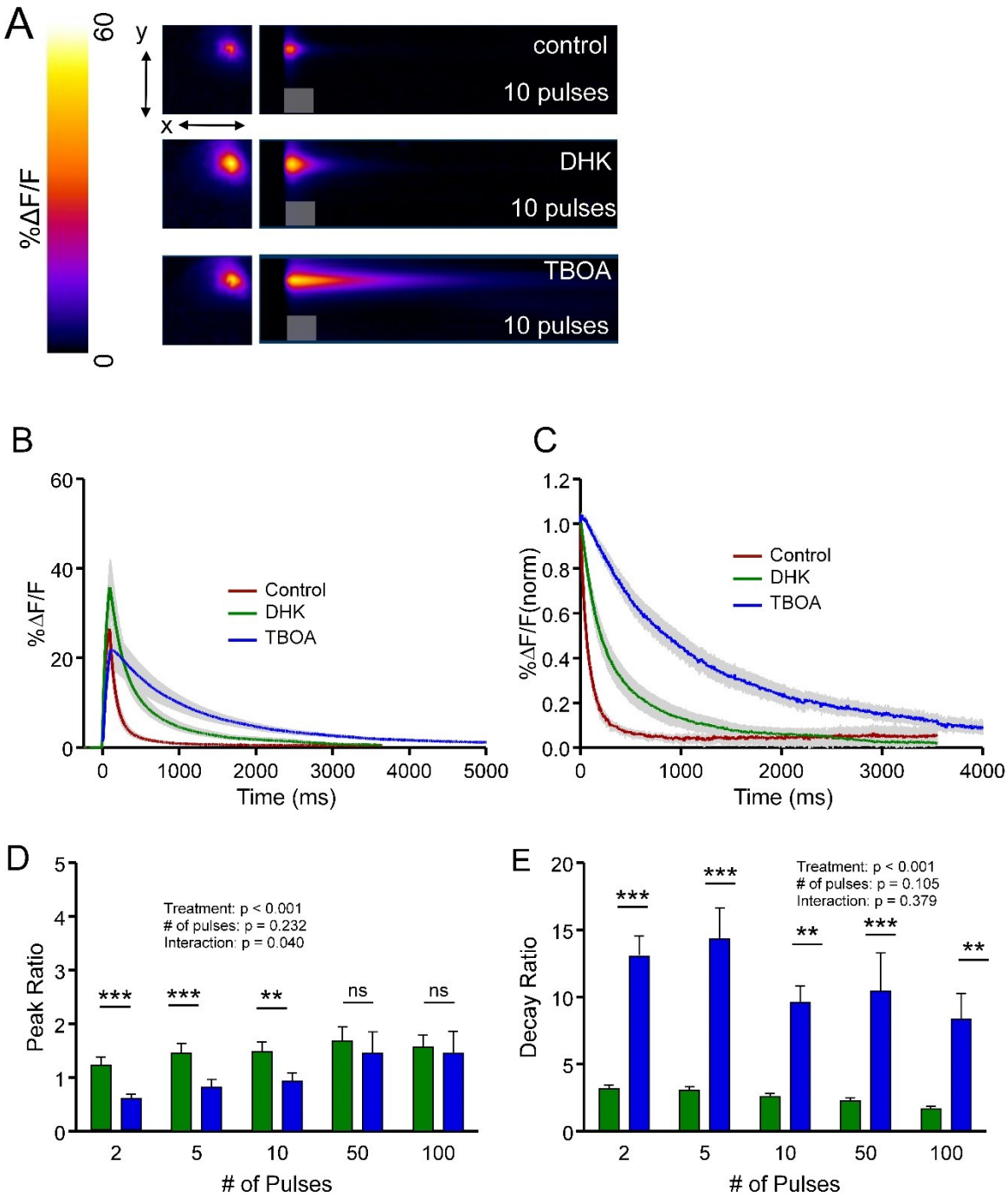
A
60
0
%ΔF/F
y
x
control
10 pulses
DHK
10 pulses
TBOA
10 pulses
B
%ΔF/F
Control
DHK
TBOA
Time (ms)
C
%ΔF/F(norm)
Control
DHK
TBOA
Time (ms)
D
Peak Ratio
Treatment: p < 0.001
# of pulses: p = 0.232
Interaction: p = 0.040
***
***
**
ns
ns
# of Pulses
E
Decay Ratio
Treatment: p < 0.001
# of pulses: p = 0.105
Interaction: p = 0.379
***
***
**
***
**
# of Pulses

Figure 21: Comparison of the effects of selective GLT-1 inhibition and nonselective transporter inhibition on glutamate dynamics in the striatum. ***A***, Representative heatmaps of striatum iGluSnFR responses after afferent stimulation (10 pulses at 100 Hz) in control conditions and after GLT-1 blockade with DHK (300 μM) and nonselective glutamate transporter blockade with TBOA (100 μM). Peak responses are shown in the *x*–*y* plane (image size, 2*2 mm), and the *y*–*z* (time) plots show the kinetics of the response at a defined *x*-coordinate adjacent to the site of stimulation (image represents 2 s). The gray shaded area within the images denotes the onset and duration of afferent stimulation. ***B***, Mean (±SEM) iGluSnFR response profiles to 10 pulses of afferent stimulation at 100 Hz in control, DHK, and TBOA conditions. ***C***, Mean responses (±SEM) from ***B*** that were normalized to the peak value at the end of the stimulation. ***D–E***, Grouped data showing mean (±SEM) DHK and TBOA peak ratios (***D***) and decay ratios (***E***) over a variety of stimulation paradigms. Peak and decay ratios indicate the fold effect of drug treatment over control levels. Two-way RM ANOVA with Bonferroni's *post hoc* results are indicated by $^{**}p < 0.01$ and $^{***}p < 0.001$.

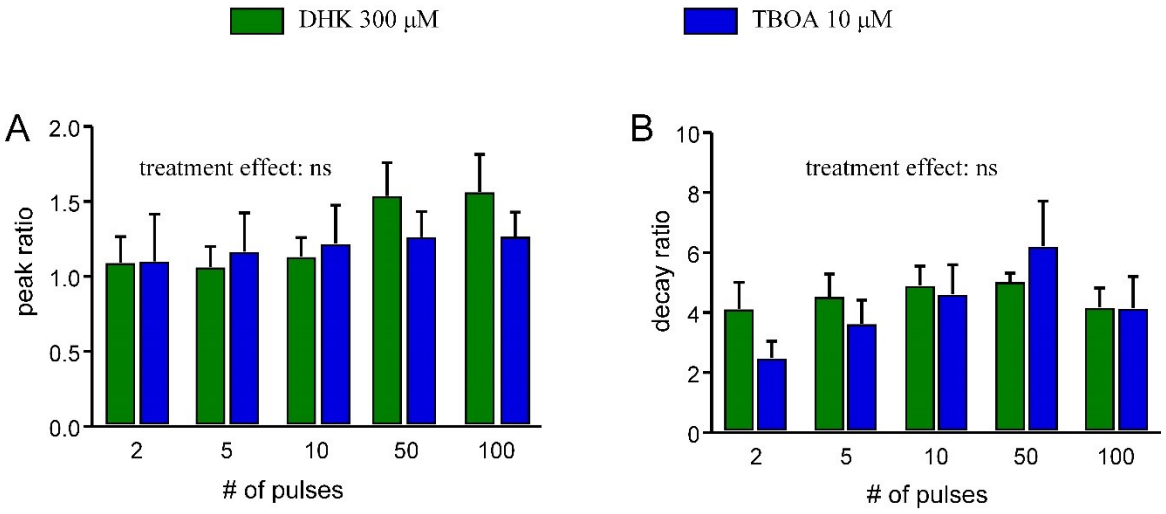

Figure 22: Comparison of the effects of selective GLT-1 inhibition and nonselective transporter inhibition on glutamate dynamics in the striatum. Grouped data showing mean (± SEM) DHK and TBOA peak ratios ***(A)*** and decay ratios ***(B)*** in cortex over a variety of stimulation paradigms while applying 300 µM DHK and 10 µM TBOA. Two way ANOVA showed non-significant treatment effect between 300 µM DHK and 10 µM TBOA.

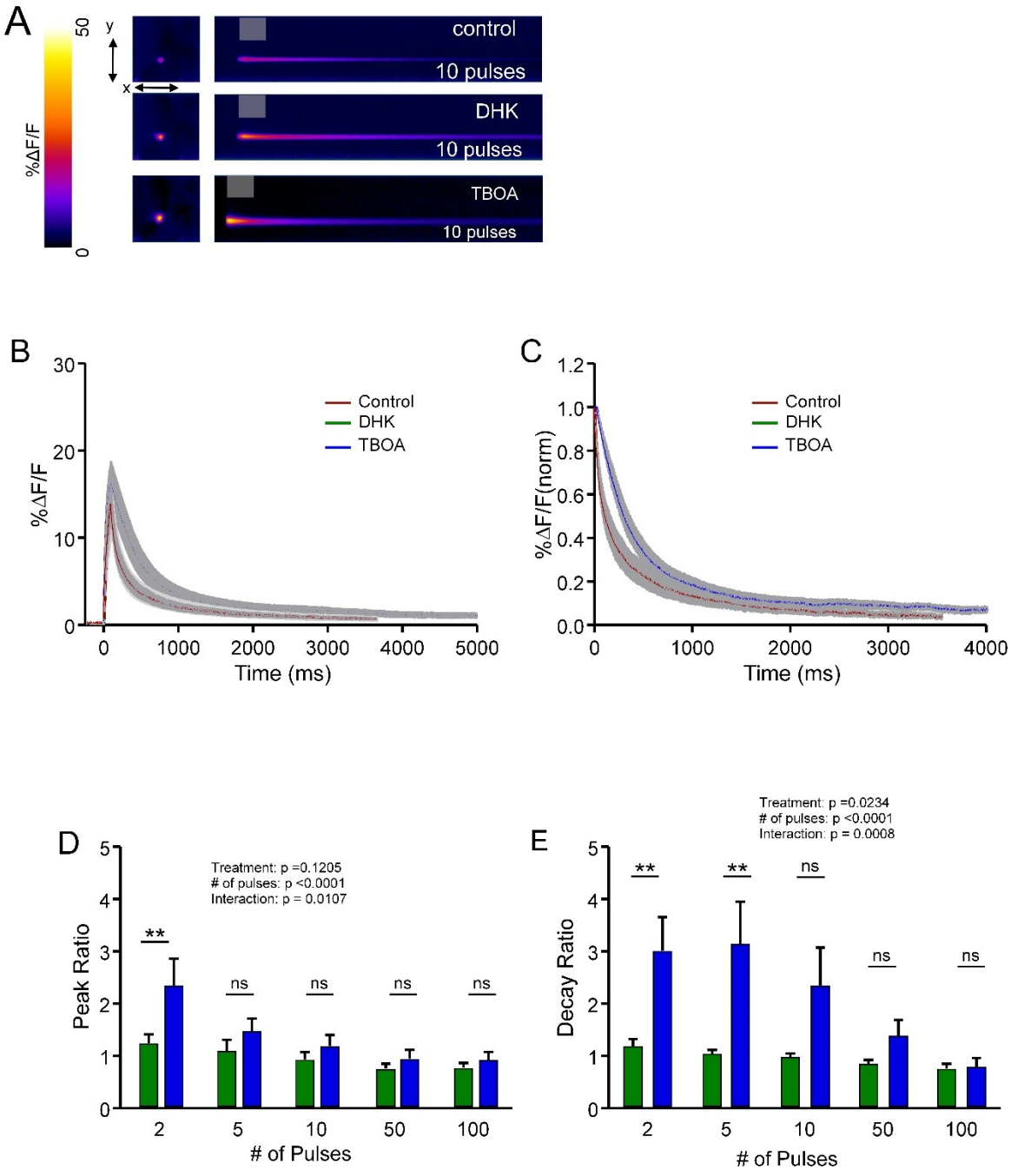
A
50
0
%ΔF/F
y
x
control
10 pulses
DHK
10 pulses
TBOA
10 pulses
B
%ΔF/F
Control
DHK
TBOA
Time (ms)
C
%ΔF/F(norm)
Control
DHK
TBOA
Time (ms)
D
Peak Ratio
Treatment: p =0.1205
# of pulses: p <0.0001
Interaction: p = 0.0107
**
ns
# of Pulses
E
Decay Ratio
Treatment: p =0.0234
# of pulses: p <0.0001
Interaction: p = 0.0008
**
**
ns
ns
ns
# of Pulses

Figure 23: Comparison of the effects of selective GLT-1 inhibition and nonselective transporter inhibition on glutamate dynamics in the cerebellum. ***A***, Representative heatmaps of cerebellum iGluSnFR responses after afferent stimulation (10 pulses at 100 Hz) in control conditions and after GLT-1 blockade with DHK (300 μM) and nonselective glutamate transporter blockade with TBOA (100 μM). Peak responses are shown in the *x–y* plane (image size, 2*2 mm), and the *y–z* (time) plots show the kinetics of the response at a defined *x*-coordinate adjacent to the site of stimulation (image represents 2 s). The gray shaded area within the images denotes the onset and duration of afferent stimulation. ***B***, Mean (±SEM) iGluSnFR response profiles to 10 pulses of afferent stimulation at 100 Hz in control, DHK, and TBOA conditions. ***C***, Mean responses (±SEM) from ***B*** that were normalized to the peak value at the end of the stimulation. ***D–E***, Grouped data showing mean (±SEM) DHK and TBOA peak ratios (***D***) and decay ratios (***E***) over a variety of stimulation paradigms. Peak and decay ratios indicate the fold effect of drug treatment over control levels. Two-way RM ANOVA with Bonferroni's *post hoc* results are indicated by $^{**}p < 0.01$.

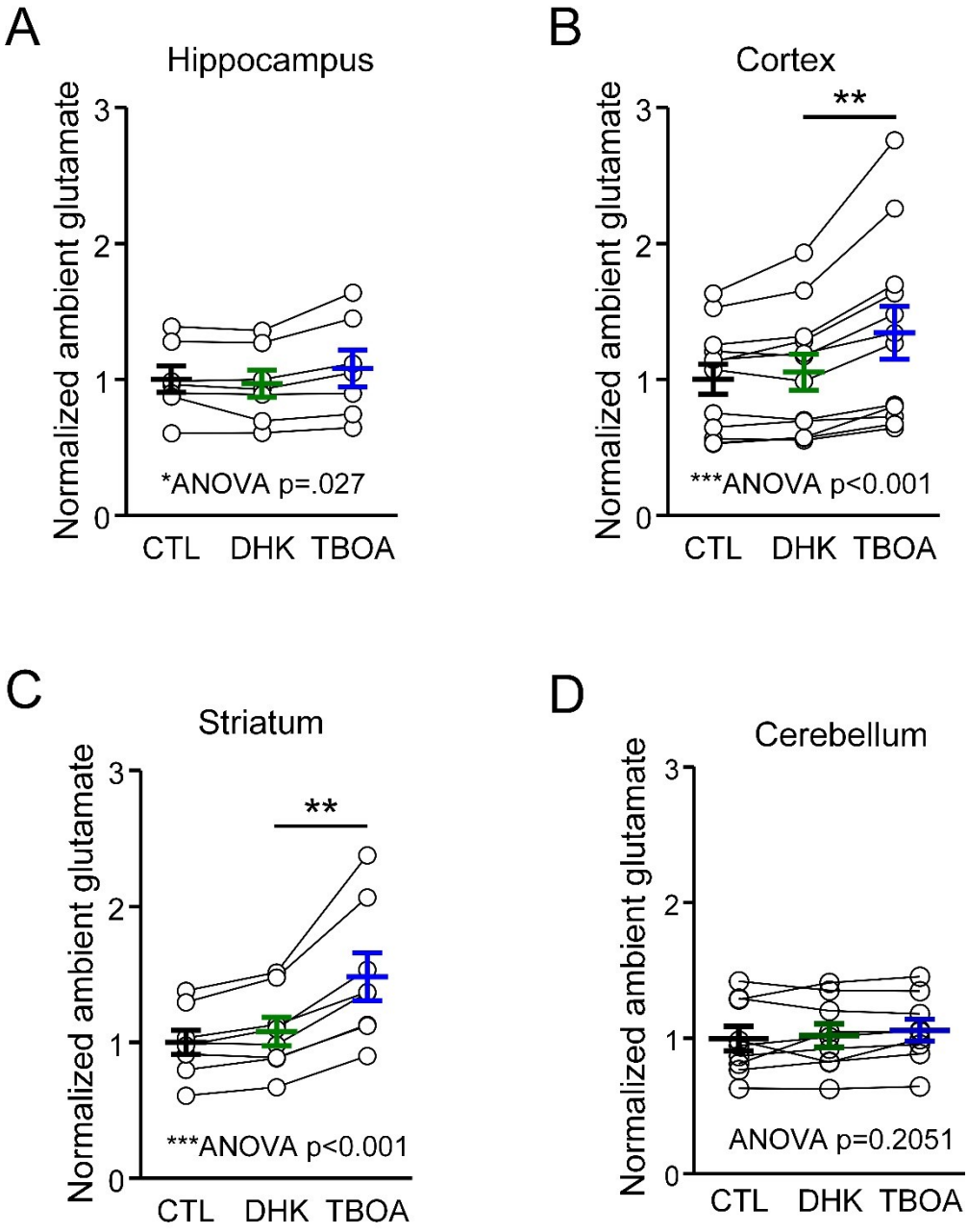
A
Hippocampus
Normalized ambient glutamate
3
2
1
0
*ANOVA p=.027
CTL DHK TBOA
B
Cortex
**
Normalized ambient glutamate
3
2
1
0
***ANOVA p<0.001
CTL DHK TBOA
C
Striatum
**
Normalized ambient glutamate
3
2
1
0
***ANOVA p<0.001
CTL DHK TBOA
D
Cerebellum
Normalized ambient glutamate
3
2
1
0
ANOVA p=0.2051
CTL DHK TBOA

Figure 24: Ambient glutamate levels after the application of DHK and TBOA. ***A–D***, Basal, unstimulated iGluSnFR fluorescence in control conditions and after GLT-1 inhibition with 300 μM DHK and nonselective glutamate transporter inhibition with 100 μM TBOA in the hippocampus (***A***), cortex (***B***), striatum (***C***) and cerebellum ***(D)***. One-way RM ANOVA significance was observed for hippocampus, cortex and striatum. Dunnett's test *post hoc* significance is indicated by $**p < 0.01$.

REFERENCES

Aoyama, K., Sang, W. S., Hamby, A. M., Liu, J., Wai, Y. C., Chen, Y., & Swanson, R. A. (2006). Neuronal glutathione deficiency and age-dependent neurodegeneration in the EAAC1 deficient mouse. *Nature Neuroscience*, *9*(1), 119–126. https://doi.org/10.1038/nn1609

Armbruster, M., Hampton, D., Yang, Y., & Dulla, C. G. (2014). Laser-scanning astrocyte mapping reveals increased glutamate-responsive domain size and disrupted maturation of glutamate uptake following neonatal cortical freeze-lesion. *Frontiers in Cellular Neuroscience*, *8*(September), 277. https://doi.org/10.3389/fncel.2014.00277

Armbruster, M., Hanson, E., & Dulla, C. G. (2016). Glutamate Clearance Is Locally Modulated by Presynaptic Neuronal Activity in the Cerebral Cortex. *The Journal of Neuroscience*, *36*(40), 10404–10415. https://doi.org/10.1523/JNEUROSCI.2066-16.2016

Arriza, J. L., Fairman, W. A., Wadiche, J. I., Murdoch, G. H., Kavanaugh, P., & Amara, S. G. (1994). Functional Comparisons of Three Glutamate Cloned from Human Motor Cortex Transporter. *Journal of Neuroscience*, *14*(9), 5559–5569.

Backus, K. H., Kettenmann, H., & Schachner, M. (1989). Pharmacological characterization of the glutamate receptor in cultured astrocytes. *Journal of Neuroscience Research*, *22*(3), 274–282. https://doi.org/10.1002/jnr.490220307

Baker, D. A., McFarland, K., Lake, R. W., Shen, H., Tang, X. C., Toda, S., & Kalivas, P. W. (2003). Neuroadaptations in cystine-glutamate exchange underlie cocaine

relapse. *Nature Neuroscience*, *6*(7), 743–749. https://doi.org/10.1038/nn1069

Balcar, V. J., & Johnston, G. A. R. (1972). The structural specificity of the high affinity uptake of L- glutamate and L-aspartate by rat brain slices. *J.Neurochem.*, *19*(i), 2657–2666.

Bandrowski, A. E. (2002). Baseline Glutamate Levels Affect Group I and II mGluRs in Layer V Pyramidal Neurons of Rat Sensorimotor Cortex. *Journal of Neurophysiology*, *89*(3), 1308–1316. https://doi.org/10.1152/jn.00644.2002

Behrens, P. F., Franz, P., Woodman, B., Lindenberg, K. S., & Landwehrmeyer, G. B. (2002). Impaired glutamate transport and glutamate-glutamine cycling: downstream effects of the Huntington mutation. *Brain : A Journal of Neurology*, *125*(Pt 8), 1908–1922.

Berger, V. U., & Hediger, A. M. (1998). Comparative analysis of glutamate transporter expression in rat brain using differential double in situ hybridization. *Anatomy and Embryology*, *198*(1), 13–30. https://doi.org/10.1007/s004290050161

Bergles, D. E., Dzubay, J. a, & Jahr, C. E. (1997). Glutamate transporter currents in bergmann glial cells follow the time course of extrasynaptic glutamate. *Proceedings of the National Academy of Sciences of the United States of America*, *94*(26), 14821–5. https://doi.org/10.1073/pnas.94.26.14821

Bergles, D. E., & Jahr, C. E. (1997). Synaptic Activation of Glutamate Transporters in Hippocampal Astrocytes, *19*, 1297–1308.

Brew, H., & Attwell, D. (1987). Electrogenic glutamate uptake is a major current carrier in the membrane of axolotl retinal glial cells. *Nature*, *327*, 707–709. https://doi.org/10.1038/327707a0

Chai, H., Diaz-Castro, B., Shigetomi, E., Monte, E., Octeau, J. C., Yu, X., … Khakh, B. S. (2017). Neural Circuit-Specialized Astrocytes: Transcriptomic, Proteomic, Morphological, and Functional Evidence. *Neuron*, *95*(3), 531–549.e9. https://doi.org/10.1016/j.neuron.2017.06.029

Christensen, H., & Fonnum, F. (1992). The ontogeny of the uptake systems for glutamate, GABA, and glycine in synaptic vesicles isolated from rat brain. *Neurochem.Res.*, *17*(5), 457–462.

Clark, B. A., & Barbour, B. (1997). Currents evoked in Bergmann glial cells by parallel fibre stimulation in rat cerebellar slices. *Journal of Physiology*, *502*(2), 335–350. https://doi.org/10.1111/j.1469-7793.1997.335bk.x

Clements, J. D. (1996). Transmitter timecourse in the synaptic cleft: Its role in central synaptic function. *Trends in Neurosciences*, *19*(5), 163–171. https://doi.org/10.1016/S0166-2236(96)10024-2

Clements, J. D., Feltz, A., Sahara, Y., & Westbrook, G. L. (1998). Activation kinetics of AMPA receptor channels reveal the number of functional agonist binding sites. *The Journal of Neuroscience : The Official Journal of the Society for Neuroscience*, *18*(1), 119–27. Retrieved from http://www.jneurosci.org/content/18/1/119.abstract

Colquhoun, D., Jonas, P., & Sakmann, B. (1992). Action of brief pulses of glutamate on AMPA/kainate receptors in patches from different neurones of rat hippocampal slices. *The Journal of Physiology*, *458*(1), 261–287. https://doi.org/10.1113/jphysiol.1992.sp019417

Cousin, M. A., & Robinson, P. J. (1999). Mechanisms of synaptic vesicle recycling illuminated by fluorescent dyes. *Journal of Neurochemistry*, *73*(6), 2227–2239.

https://doi.org/10.1046/j.1471-4159.1999.0732227.x

Currie, D. N., & Kelly, J. S. (1981). Glial versus neuronal uptake of glutamate. *The Journal of Experimental Biology*, *95*, 181–193.

Curtis, D. R., & Johnston, G. A. (1974). Amino acid transmitters in the mammalian central nervous system. *Ergebnisse Der Physiologie, Biologischen Chemie Und Experimentellen Pharmakologie*, *69*(0), 97–188.

Curtis, D. R., Lodge, D., & McLennan, H. (1979). The excitation and depression of spinal neurones by ibotenic acid. *The Journal of Physiology*, *291*(1), 19–28. https://doi.org/10.1113/jphysiol.1979.sp012796

CURTIS, D. R., PHILLIS, J. W., & WATKINS, J. C. (1961). Actions of Amino- Acids on the Isolated Hemisected Spinal Cord of the Toad. *British Journal of Pharmacology and Chemotherapy*, *16*(3), 262–283. https://doi.org/10.1111/j.1476-5381.1961.tb01086.x

Danbolt, N. C., Furness, D. N., & Zhou, Y. (2016). Neuronal vs glial glutamate uptake: Resolving the conundrum. *Neurochemistry International*, *98*, 29–45. https://doi.org/10.1016/j.neuint.2016.05.009

Danbolt, N. C. N. C. (2001). Glutamate uptake. *Progress in Neurobiology*, *65*(1), 1–105. Retrieved from http://www.sciencedirect.com/science/article/pii/S0301008200000678

Danbolt, N. C., Pines, G., & Kanner, B. I. (1990). Purification and Reconstitution of the Sodium- and Potassium-Coupled Glutamate Transport Glycoprotein from Rat Brain. *Biochemistry*, *29*(28), 6734–6740. https://doi.org/10.1021/bi00480a025

Danbolt, N. C., Storm-Mathisen, J., & Kanner, B. I. (1992). An [Na+ + K+]coupled l-

glutamate transporter purified from rat brain is located in glial cell processes. *Neuroscience*, *51*(2), 295–310. https://doi.org/10.1016/0306-4522(92)90316-T

Day, B. K., Pomerleau, F., Burmeister, J. J., Huettl, P., & Gerhardt, G. A. (2006). Microelectrode array studies of basal and potassium-evoked release of L-glutamate in the anesthetized rat brain. *Journal of Neurochemistry*, *96*(6), 1626–1635. https://doi.org/10.1111/j.1471-4159.2006.03673.x

Dehnes, Y., Chaudhry, F. A., Ullensvang, K., Lehre, K. P., Storm-Mathisen, J., & Danbolt, N. C. (1998). The glutamate transporter EAAT4 in rat cerebellar Purkinje cells: a glutamate-gated chloride channel concentrated near the synapse in parts of the dendritic membrane facing astroglia. *The Journal of Neuroscience : The Official Journal of the Society for Neuroscience*, *18*(10), 3606–19.

Diamond, J. S. (2005). Deriving the Glutamate Clearance Time Course from Transporter Currents in CA1 Hippocampal Astrocytes: Transmitter Uptake Gets Faster during Development. *Journal of Neuroscience*, *25*(11), 2906–2916. https://doi.org/10.1523/JNEUROSCI.5125-04.2005

Diamond, J. S., & Jahr, C. E. (1997). Transporters Buffer Synaptically Released Glutamate on a Submillisecond Time Scale, *17*(12), 4672–4687.

Diamond, J. S., & Jahr, C. E. (2000). Synaptically released glutamate does not overwhelm transporters on hippocampal astrocytes during high-frequency stimulation. *Journal of Neurophysiology*, *83*(5), 2835–43. https://doi.org/10.1101/cshperspect.a006262

Diamond, J. S., & Jahr, C. E. (2000). Synaptically Released Glutamate Does Not Overwhelm Transporters on Hippocampal Astrocytes During High-Frequency

Stimulation, 2835–2843.

Dodd, P. R., Hardy, J. A., Oakley, A. E., Edwardson, J. A., Perry, E. K., & Delaunoy, J. P. (1981). A rapid method for preparing synaptosomes: Comparison, with alternative procedures. *Brain Research*, *226*(1–2), 107–118. https://doi.org/10.1016/0006-8993(81)91086-6

Dore, X. K., Stein, I. S., Brock, X. J. A., Castillo, X. P. E., Zito, X. K., & Sjo, X. P. J. (2017). Unconventional NMDA Receptor Signaling, *37*(45), 10800–10807. https://doi.org/10.1523/JNEUROSCI.1825-17.2017

Drejer, J., Larsson, O. M., & Schousboe, A. (1982). Characterization of L-glutamate uptake into and release from astrocytes and neurons cultured from different brain regions. *Experimental Brain Research*, *47*(2), 259–269.

Dzubay, J. a, & Jahr, C. E. (1996). Kinetics of NMDA channel opening. *The Journal of Neuroscience : The Official Journal of the Society for Neuroscience*, *16*(13), 4129–34. Retrieved from http://www.ncbi.nlm.nih.gov/pubmed/8753874

Dzubay, J. a, & Jahr, C. E. (1999). The concentration of synaptically released glutamate outside of the climbing fiber-Purkinje cell synaptic cleft. *The Journal of Neuroscience : The Official Journal of the Society for Neuroscience*, *19*(13), 5265–5274.

Fairman, W. A., Vandenberg, R. J., Arriza, J. L., Kavanaught, M. P., & Amara, S. G. (1995). An excitatory amino-acid transporter with properties of a ligand-gated chloride channel. *Nature*. https://doi.org/10.1038/375599a0

Fonnum, F. (1984). Glutamate: A Neurotransmitter in Mammalian Brain. *Journal of Neurochemistry*, *42*(1), 1–11. https://doi.org/10.1111/j.1471-4159.1984.tb09689.x

Foster, K. A., Kreitzer, A. C., & Regehr, W. G. (2002). Interaction of postsynaptic receptor saturation with presynaptic mechanisms produces a reliable synapse. *Neuron*, *36*(6), 1115–1126. https://doi.org/10.1016/S0896-6273(02)01106-6

Ginsberg, S. D., Martin, L. J., & Rothstein, J. D. (1995). Regional deafferentation down-regulates subtypes of glutamate transporter proteins. *Journal of Neurochemistry*, *65*(6), 2800–3. https://doi.org/10.1046/j.1471-4159.1995.65062800.x

Gladding, C. M., & Raymond, L. A. (2011). Mechanisms underlying NMDA receptor synaptic/extrasynaptic distribution and function. *Molecular and Cellular Neuroscience*, *48*(4), 308–320. https://doi.org/10.1016/j.mcn.2011.05.001

Glaum, S. R., Holzwarth, J. A., & Miller, R. J. (1990). Glutamate receptors activate Ca2+ mobilization and Ca2+ influx into astrocytes. *Proceedings of the National Academy of Sciences of the United States of America*, *87*(9), 3454–8. https://doi.org/10.1073/pnas.87.9.3454

Greger, I. H., Ziff, E. B., & Penn, A. C. (2007). Molecular determinants of AMPA receptor subunit assembly. *Trends in Neurosciences*, *30*(8), 407–416. https://doi.org/10.1016/j.tins.2007.06.005

Grewer, C., & Rauen, T. (2005). Electrogenic glutamate transporters in the CNS: Molecular mechanism, pre-steady-state kinetics, and their impact on synaptic signaling. *Journal of Membrane Biology*. https://doi.org/10.1007/s00232-004-0731-6

Hanson, E., Armbruster, M., Cantu, D., Andresen, L., Taylor, A., Danbolt, N. C., & Dulla, C. G. (2015). Astrocytic glutamate uptake is slow and does not limit neuronal NMDA receptor activation in the neonatal neocortex. *Glia*, *63*(10), 1784–96. https://doi.org/10.1002/glia.22844

Hardingham, G. E., & Bading, H. (2010). Synaptic versus extrasynaptic NMDA receptor signalling: implications for neurodegenerative disorders. *Nature Reviews. Neuroscience*, *11*(10), 682–96. article. https://doi.org/10.1038/nrn2911

Haugeto, O., Ullensvang, K., Levy, L. M., Chaudhry, F. a., Honore, T., Nielsen, M., … Honoré, T. (1996). Brain Glutamate Transporter Proteins Form Homomultimers. *Journal of Biological Chemistry*, *271*(44), 27715–27722. https://doi.org/10.1074/jbc.271.44.27715

Herman, M. A., & Jahr, C. E. (2007). Extracellular Glutamate Concentration in Hippocampal Slice. *Journal of Neuroscience*, *27*(36), 9736–9741. https://doi.org/10.1523/JNEUROSCI.3009-07.2007

Hestrin, S. (1992). Activation and desensitization of glutamate-activated channels mediating fast excitatory synaptic currents in the visual cortex. *Neuron*, *9*(5), 991–999. https://doi.org/10.1016/0896-6273(92)90250-H

Holmseth, S., Dehnes, Y., Huang, Y. H., Follin-Arbelet, V. V., Grutle, N. J., Mylonakou, M. N., … Danbolt, N. C. (2012). The Density of EAAC1 (EAAT3) Glutamate Transporters Expressed by Neurons in the Mammalian CNS. *Journal of Neuroscience*, *32*(17), 6000–6013. https://doi.org/10.1523/JNEUROSCI.5347-11.2012

Horak, F. B., Nashner, L. M., & Diener, H. C. (1990). Characterization of glutamate uptake into and release from astrocytes and neurons cultured from different brain regions. *Experimental Brain Research*, *47*(2), 167–177. https://doi.org/10.1007/BF00239385

Howland, D. S., Liu, J., She, Y., Goad, B., Maragakis, N. J., Kim, B., … Rothstein, J. D.

(2002). Focal loss of the glutamate transporter EAAT2 in a transgenic rat model of SOD1 mutant-mediated amyotrophic lateral sclerosis (ALS). *Proceedings of the National Academy of Sciences*, *99*(3), 1604–1609. https://doi.org/10.1073/pnas.032539299

Hrabětová, S. (2005). Extracellular diffusion is fast and isotropic in the stratum radiatum of hippocampal CA1 region in rat brain slices. *Hippocampus*, *15*(4), 441–450. https://doi.org/10.1002/hipo.20068

Huang, K., Kang, M. H., Askew, C., Kang, R., Sanders, S. S., Wan, J., … Hayden, M. R. (2010). Palmitoylation and function of glial glutamate transporter-1 is reduced in the YAC128 mouse model of Huntington disease. *Neurobiology of Disease*, *40*(1), 207–215. https://doi.org/10.1016/j.nbd.2010.05.027

Hynd, M. R., Scott, H. L., & Dodd, P. R. (2004). Glutamate-mediated excitotoxicity and neurodegeneration in Alzheimer's disease. *Neurochemistry International*, *45*(5), 583–595. https://doi.org/10.1016/j.neuint.2004.03.007

Iacobucci, G. J., & Popescu, G. K. (2017). NMDA receptors: Linking physiological output to biophysical operation. *Nature Reviews Neuroscience*, *18*(4), 236–249. https://doi.org/10.1038/nrn.2017.24

Kanai, Y., & Hediger, M. A. (1992). Primary structure and functional characterization of a high-affinity glutamate transporter. *Nature*, *360*(6403), 467–71. https://doi.org/10.1038/360467a0

Kiryk, A., Aida, T., Tanaka, K., & Banerjee, P. (2008). Behavioral Characterization of GLT1 (+ / -) Mice as a Model of Mild Glutamatergic Hyperfunction, *13*(1), 19–30.

Kish, P. E., Kim, S. Y., & Ueda, T. (1989). Ontogeny of glutamate accumulating activity

in rat brain synaptic vesicles. *Neuroscience Letters*, *97*(1–2), 185–90. Retrieved from http://www.ncbi.nlm.nih.gov/pubmed/2563905

Lane, M. C., Jackson, J. G., Krizman, E. N., Rothstein, J. D., Porter, B. E., & Robinson, M. B. (2014). Genetic deletion of the neuronal glutamate transporter, EAAC1, results in decreased neuronal death after pilocarpine-induced status epilepticus. *Neurochemistry International*, *73*, 152–158. https://doi.org/10.1016/j.neuint.2013.11.013

Lehre, K. P., Levy, L. M., Ottersen, O. P., Storm-Mathisen, J., & Danbolt, N. C. (1995). Differential expression of two glial glutamate transporters in the rat brain: quantitative and immunocytochemical observations. *The Journal of Neuroscience : The Official Journal of the Society for Neuroscience*, *15*(3 Pt 1), 1835–1853. https://doi.org/10.1038/NN1623

Lester, R. A., & Jahr, C. E. (1992). NMDA channel behavior depends on agonist affinity. *The Journal of Neuroscience : The Official Journal of the Society for Neuroscience*, *12*(2), 635–43. https://doi.org/10.1523/jneurosci.6160-08.2009

Levi, G. I. U. L. I. O., & Raiteri, M. A. U. R. I. Z. I. O. (1973). G I U L I O LEVI AND M A U R I Z I O RAITERI Laboratory of Cell Biology, Via Romagnosi 18A, 00196 Rome and Institute of Pharmacology, Catholic University, Rome (Italy) (Accepted December 13th, 1972), *57*, 165–185.

Levy, L. M., Lehre, K. P., Rolstad, B., & Danbolt, N. C. (1993). A monoclonal antibody raised against an [Na+K+]coupled l-glutamate transporter purified from rat brain confirms glial cell localization. *FEBS Letters*, *317*(1–2), 79–84. https://doi.org/10.1016/0014-5793(93)81495-L

Li, S., Jin, M., Koeglsperger, T., Shepardson, N. E., Shankar, G. M., & Selkoe, D. J. (2011). Soluble A Oligomers Inhibit Long-Term Potentiation through a Mechanism Involving Excessive Activation of Extrasynaptic NR2B-Containing NMDA Receptors. *Journal of Neuroscience*, *31*(18), 6627–6638. https://doi.org/10.1523/JNEUROSCI.0203-11.2011

Liévens, J. C., Woodman, B., Mahal, a, Spasic-Boscovic, O., Samuel, D., Kerkerian-Le Goff, L., & Bates, G. P. (2001). Impaired glutamate uptake in the R6 Huntington's disease transgenic mice. *Neurobiology of Disease*, *8*(5), 807–821. https://doi.org/10.1006/nbdi.2001.0430

Liguz-Lecznar, M., & Skangiel-Kramska, J. (2007). Vesicular glutamate transporters (VGLUTs): the three musketeers of glutamatergic system. *Acta Neurobiologiae Experimentalis*, *67*(3), 207–218.

Linden, D. J. (1997). Long-Term Potentiation of Glial Synaptic Currents in Cerebellar Culture, *18*, 983–994.

Ludger, J., & Galli, T. (1998). Exocytosis: SNAREs drum up! *European Journal of Neuroscience*, *10*(2), 415–422. https://doi.org/10.1046/j.1460-9568.1998.00081.x

Marcaggi, P., Billups, D., & Attwell, D. (2003). The role of glial glutamate transporters in maintaining the independent operation of juvenile mouse cerebellar parallel fibre synapses, 89–107. https://doi.org/10.1113/jphysiol.2003.044263

Marvin, J. S., Borghuis, B. G., Tian, L., Cichon, J., Harnett, M. T., Akerboom, J., … Looger, L. L. (2013). An optimized fluorescent probe for visualizing glutamate neurotransmission. *Nature Methods*, *10*(2), 162–170. https://doi.org/10.1038/nmeth.2333

Masliah, E., Alford, M., R, D., Mallory, M., & Hansen, L. (1996). Deficient glutamate transport is associated with neurodegeneration in Alzheimer's disease. *Ann. Neurol.*, *40*(5), 759–766. article. https://doi.org/10.1002/ana.410400512

Matsugami, T. R., Tanemura, K., Mieda, M., Nakatomi, R., Yamada, K., Kondo, T., … Tanaka, K. (2006). Indispensability of the glutamate transporters GLAST and GLT1 to brain development, *103*(32), 1–5.

McLamore, E. S., Mohanty, S., Shi, J., Claussen, J., Jedlicka, S. S., Rickus, J. L., & Porterfield, D. M. (2010). A self-referencing glutamate biosensor for measuring real time neuronal glutamate flux. *Journal of Neuroscience Methods*, *189*(1), 14–22. https://doi.org/https://doi.org/10.1016/j.jneumeth.2010.03.001

Meeks, J. P., & Mennerick, S. (2007). Astrocyte membrane responses and potassium accumulation during neuronal activity. *Hippocampus*, *17*(11), 1100–1108. https://doi.org/10.1002/hipo.20344

Meldrum, B. S. (2000). Glutamate and Glutamine in the Brain Glutamate as a Neurotransmitter in the Brain : Review of Physiology, *8*, 1007–1015.

Melendez, R. I., Hicks, M. P., Cagle, S. S., & Kalivas, P. W. (2005). Ethanol exposure decreases glutamate uptake in the nucleus accumbens. *Alcoholism: Clinical and Experimental Research*, *29*(3), 326–333. https://doi.org/10.1097/01.ALC.0000156086.65665.4D

Melzer, N., Torres-Salazar, D., & Fahlke, C. (2005). A dynamic switch between inhibitory and excitatory currents in a neuronal glutamate transporter. *Proceedings of the National Academy of Sciences of the United States of America*, *102*(52), 19214–19218. https://doi.org/10.1073/pnas.0508837103

Miele, M., Berners, M., Boutelle, M. G., Kusakabe, H., & Fillenz, M. (1996). The determination of the extracellular concentration of brain glutamate using quantitative microdialysis. *Brain Research*, *707*(1), 131–133. https://doi.org/10.1016/0006-8993(95)01371-7

Miller, B. R., Dorner, J. L., Shou, M., Sari, Y., Barton, S. J., Sengelaub, D. R., … Rebec, G. V. (2008). Up-regulation of GLT1 expression increases glutamate uptake and attenuates the Huntington's disease phenotype in the R6/2 mouse. *Neuroscience*, *153*(1), 329–337. https://doi.org/10.1016/j.neuroscience.2008.02.004

Milnerwood, A. J., Gladding, C. M., Pouladi, M. A., Kaufman, A. M., Hines, R. M., Boyd, J. D., … Raymond, L. A. (2010). Early Increase in Extrasynaptic NMDA Receptor Signaling and Expression Contributes to Phenotype Onset in Huntington's Disease Mice. *Neuron*, *65*(2), 178–190. https://doi.org/10.1016/j.neuron.2010.01.008

Morgan, J. (1971). © 1971 Nature Publishing Group. *Nature*, *233*(October 27 1971), 267–268.

Moussawi, K., Riegel, A., Nair, S., & Kalivas, P. W. (2011). Extracellular Glutamate: Functional Compartments Operate in Different Concentration Ranges. *Frontiers in Systems Neuroscience*, *5*(November), 1–9. https://doi.org/10.3389/fnsys.2011.00094

Naito, S., & Ueda, T. (1983). Adenosine triphosphate-dependent uptake of glutamate into protein I-associated synaptic vesicles. *Journal of Biological Chemistry*, *258*(2), 696–699.

Nakanishi, S., Masu, M., Bessho, Y., Nakajima, Y., Hayashi, Y., & Shigemoto, R. (1994). Molecular diversity of glutamate receptors and their physiological functions. *EXS*, *71*, 71–80. Retrieved from http://0.122.143.174

Nicholson, C., Kamali-Zare, P., & Tao, L. (2011). Brain extracellular space as a diffusion barrier. *Computing and Visualization in Science*, *14*(7), 309–325. https://doi.org/10.1007/s00791-012-0185-9

Nicholson, C., & Sykova, E. (1998). Extracellular space structure revealed by diffusion analysis.[see comment]. *Trends in Neurosciences.*, *21*(5), 207–215. https://doi.org/10.1016/S0166-2236(98)01261-2

Nicholson, C., & Tao, L. (1993). Hindered diffusion of high molecular weight compounds in brain extracellular microenvironment measured with integrative optical imaging. *Biophysical Journal*, *65*(6), 2277–2290. https://doi.org/10.1016/S0006-3495(93)81324-9

Niswender, C. M., & Conn, P. J. (2010). Metabotropic Glutamate Receptors: Physiology, Pharmacology, and Disease. *Annu Rev Pharmacol Toxicol*, *50*, 295–322. https://doi.org/10.1146/annurev.pharmtox.011008.145533.Metabotropic

Okamoto, S., Pouladi, M. a, Talantova, M., Yao, D., Xia, P., Ehrnhoefer, D. E., … Lipton, S. a. (2009). Balance between synaptic versus extrasynaptic NMDA receptor activity influences inclusions and neurotoxicity of mutant huntingtin. *Nature Medicine*, *15*(12), 1407–1413. https://doi.org/10.1038/nm.2056

Oldenziel, W. H., van der Zeyden, M., Dijkstra, G., Ghijsen, W. E. J. M., Karst, H., Cremers, T. I. F. H., & Westerink, B. H. C. (2007). Monitoring extracellular glutamate in hippocampal slices with a microsensor. *Journal of Neuroscience Methods*, *160*(1), 37–44. https://doi.org/10.1016/j.jneumeth.2006.08.003

Oliet, S. H. R. (2001). Control of Glutamate Clearance and Synaptic Efficacy by Glial Coverage of Neurons. *Science*, *292*(May), 923–927.

https://doi.org/10.1126/science.1059162

Otis, T. S., & Kavanaugh, M. P. (2000). Isolation of Current Components and Partial Reaction Cycles in the Glial Glutamate Transporter EAAT2, *20*(8), 2749–2757.

Otis, T. S., Michael P. Kavanaugh, & Craig E. Jahr. (1997). Synapse Postsynaptic Glutamate Transport at the Climbing Fiber – Purkinje Cell Synapse. *Science*, *1515*(1997), 1–5. https://doi.org/10.1126/science.277.5331.1515

Ottersen, O. P., Laake, J. H., Reichelt, W., Haug, F. M., & Torp, R. (1996). Ischemic disruption of glutamate homeostasis in brain: Quantitative immunocytochemical analyses. *Journal of Chemical Neuroanatomy*, *12*(1), 1–14. https://doi.org/10.1016/S0891-0618(96)00178-0

Ottersen, O. P., & Storm-Mathisen, J. (1984). Glutamate- and gaba-containing neurons in the mouse and rat brain, as demonstrated with a mew immunocytochemical technique. *J. of Comparative Neurology*, *229*, 374–392.

Ottersen, O. P., Zhang, N., & Walberg, F. (1992). Metabolic compartmentation of glutamate and glutamine: Morphological evidence obtained by quantitative immunocytochemistry in rat cerebellum. *Neuroscience*, *46*(3), 519–534. https://doi.org/10.1016/0306-4522(92)90141-N

Paoletti, P., Bellone, C., & Zhou, Q. (2013). NMDA receptor subunit diversity: Impact on receptor properties, synaptic plasticity and disease. *Nature Reviews Neuroscience*, *14*(6), 383–400. https://doi.org/10.1038/nrn3504

Parsons, M. P., & Raymond, L. A. (2014). Review Extrasynaptic NMDA Receptor Involvement in Central Nervous System Disorders. *Neuron*, *82*(2), 279–293. https://doi.org/10.1016/j.neuron.2014.03.030

Parsons, M. P., Vanni, M. P., Woodard, C. L., Kang, R., Murphy, T. H., & Raymond, L. A. (2016). Real-time imaging of glutamate clearance reveals normal striatal uptake in Huntington disease mouse models. *Nature Communications*, *7*, 1–12. https://doi.org/10.1038/ncomms11251

Perea, G., Navarrete, M., & Araque, A. (2009). Tripartite synapses: astrocytes process and control synaptic information. *Trends in Neurosciences*, *32*(8), 421–431. article. https://doi.org/10.1016/j.tins.2009.05.001

Petr, G. T., Sun, Y., Frederick, N. M., Zhou, Y., Dhamne, S. C., Hameed, M. Q., … Rosenberg, P. A. (2015). Conditional deletion of the glutamate transporter GLT-1 reveals that astrocytic GLT-1 protects against fatal epilepsy while neuronal GLT-1 contributes significantly to glutamate uptake into synaptosomes. *The Journal of Neuroscience : The Official Journal of the Society for Neuroscience*, *35*(13), 5187–201. https://doi.org/10.1523/JNEUROSCI.4255-14.2015

Pines, G., & Danbolt NC, Bjørås M, Zhang Y, Bendahan A, Eide L, Koepsell H, Storm-Mathisen J, Seeberg E, K. B. (1992). Cloning and expression of a rat brain L-glutamate transporter. *Nature*, *360*(6403), 464–467. https://doi.org/10.1038/360464a0

Pinky, N. F., Wilkie, C. M., Barnes, J. R., & Parsons, M. P. (2018). Region- and activity-dependent regulation of extracellular glutamate. *The Journal of Neuroscience*, *38*(23), 3213–17. https://doi.org/10.1523/JNEUROSCI.3213-17.2018

Pisani, A., Calabresi, P., Centonze, D., & Bernardi, G. (1997). Activation of group III metabotropic glutamate receptors depresses glutamatergic transmission at corticostriatal synapse. *Neuropharmacology*, *36*(6), 845–851.

https://doi.org/10.1016/S0028-3908(96)00177-3

Raiteri, L., & Raiteri, M. (2000). Synaptosomes still viable after 25 years of superfusion. *Neurochemical Research*, *25*(9–10), 1265–74. https://doi.org/10.1023/A:1007648229795

Rothstein, J. D., Martin, L., Levey, A. I., Dykes-Hoberg, M., Jin, L., Wu, D., … Kuncl, R. W. (1994). Localization of neuronal and glial glutamate transporters. *Neuron*, *13*(3), 713–725. https://doi.org/10.1016/0896-6273(94)90038-8

Rothstein, J. D., Van Kammen, M., Levey, a I., Martin, L. J., & Kuncl, R. W. (1995). Selective loss of glial glutamate transporter GLT-1 in amyotrophic lateral sclerosis. *Annals of Neurology*, *38*(1), 73–84. https://doi.org/10.1002/ana.410380114

Sarantis, M., Ballerini, L., Miller, B., Silver, R. A., Edwards, M., & Attwell, D. (1993). Glutamate uptake from the synaptic cleft does not shape the decay of the non-NMDA component of the synaptic current. *Neuron*, *11*(3), 541–549. https://doi.org/10.1016/0896-6273(93)90158-N

Schmidt, W., Wolf, G., & Republic, G. D. (1988). Exp.er_imental Brain Research 9, 50–54.

Schmitt, A., Asan, E., Pü, B., & Kugler, P. (1997). Cellular and Regional Distribution of the Glutamate Transporter GLAST in the CNS of Rats: Nonradioactive In Situ Hybridization and Comparative Immunocytochemistry. *The Journal of N*, *17*(1), 1–10.

Schwartz, E. A., & Tachibana, M. (1990). Electrophysiology of glutamate and sodium co???transport in a glial cell of the salamander retina. *The Journal of Physiology*, *426*(1), 43–80. https://doi.org/10.1113/jphysiol.1990.sp018126

Scott, H. A., Gebhardt, F. M., Mitrovic, A. D., Vandenberg, R. J., & Dodd, P. R. (2011). Glutamate transporter variants reduce glutamate uptake in Alzheimer's disease. *Neurobiology of Aging*, *32*(3). https://doi.org/10.1016/j.neurobiolaging.2010.03.008

Shashidharan, P., Huntley, G. W., Murray, J. M., Buku, A., Moran, T., Walsh, M. J., … Plaitakis, A. (1997). Immunohistochemical localization of the neuron-specific glutamate transporter EAAC1 (EAAT3) in rat brain and spinal cord revealed by a novel monoclonal antibody. *Brain Research*, *773*(1–2), 139–148. https://doi.org/10.1016/S0006-8993(97)00921-9

Song, I., & Huganir, R. L. (2002). Regulation of AMPA receptors during synaptic plasticity.pdf. *Trends in Neurosciences*, *25*(11), 578–588. https://doi.org/S0166223602022701

Sontheimer, H., Kettenmann, H., Backus, K. H., & Schachner, M. (1988). Glutamate opens Na+/K+ channels in cultured astrocytes. *Glia*, *1*(5), 328–36. https://doi.org/10.1002/glia.440010505

Stoffel, W. (1997). Northern blot hybridization analysis. Polymerase chain. *The EMBO Journal Pines et Al*, *16*(13), 3822–3832. https://doi.org/10.1093/emboj/16.13.3822

Sung, K. W., Choi, S., & Lovinger, D. M. (2001). Activation of group I mGluRs is necessary for induction of long-term depression at striatal synapses. *J Neurophysiol*, *86*(5), 2405–2412.

Syková, E., Nicholson, C., & Sykova, Eva; Nicholson, C. (2008). Diffusion in brain extracellular space. *Physiological Reviews*, *88*(4), 1277–1340. https://doi.org/10.1152/physrev.00027.2007.Diffusion

Sykova, E., Vargova, L., Prokopova, S., & Simonova, Z. (1999). Glial swelling and

astrogliosis produce diffusion barriers in the rat spinal cord. *Glia*, *25*(1), 56–70.

Takayasu, Y., Iino, M., Kakegawa, W., Maeno, H., Watase, K., Wada, K., … Ozawa, S. (2005). Differential roles of glial and neuronal glutamate transporters in Purkinje cell synapses. *The Journal of Neuroscience : The Official Journal of the Society for Neuroscience*, *25*(38), 8788–8793. https://doi.org/10.1523/JNEUROSCI.1020-05.2005

Tanaka, K., Watase, K., Manabe, T., Yamada, K., Watanabe, M., Takahashi, K., … Wada, K. (1997). Epilepsy and exacerbation of brain injury in mice lacking the glutamate transporter GLT-1. *Science (New York, N.Y.)*, *276*(5319), 1699–1702.

Thomas, C. G., Tian, H., & Diamond, J. S. (2011). The Relative Roles of Diffusion and Uptake in Clearing Synaptically Released Glutamate Change during Early Postnatal Development, *31*(12), 4743–4754. https://doi.org/10.1523/JNEUROSCI.5953-10.2011

Thomas, C. G., Tian, H., & Diamond, J. S. (2011). The Relative Roles of Diffusion and Uptake in Clearing Synaptically Released Glutamate Change during Early Postnatal Development. *Journal of Neuroscience*, *31*(12), 4743–4754. https://doi.org/10.1523/JNEUROSCI.5953-10.2011

Traynelis, S. F., Wollmuth, L. P., McBain, C. J., Menniti, F. S., Vance, K. M., Ogden, K. K., … Dingledine, R. (2010). Glutamate receptor ion channels: structure, regulation, and function. *Pharmacological Reviews*. https://doi.org/10.1124/pr.109.002451

Tzingounis, A. V., & Wadiche, J. I. (2007). Glutamate transporters: Confining runaway excitation by shaping synaptic transmission. *Nature Reviews Neuroscience*, *8*(12), 935–947. https://doi.org/10.1038/nrn2274

Ullensvang, K., Lehre, K. P., & Danbolt, N. C. (1997). Differential Developmental Expression of the Two Rat Brain Glutamate Transporter Proteins GLAST and GLT, *9*, 1646–1655.

Van Den Bosch, L., Van Damme, P., Bogaert, E., & Robberecht, W. (2006). The role of excitotoxicity in the pathogenesis of amyotrophic lateral sclerosis. *Biochimica et Biophysica Acta - Molecular Basis of Disease*, *1762*(11–12), 1068–1082. https://doi.org/10.1016/j.bbadis.2006.05.002

Vandenberg, R. J., & Ryan, R. M. (2013). Mechanisms of glutamate transport. *Physiological Reviews*, *93*(4), 1621–57. https://doi.org/10.1152/physrev.00007.2013

Veruki, M. L., Mørkve, S. H., & Hartveit, E. (2006). Activation of a presynaptic glutamate transporter regulates synaptic transmission through electrical signaling. *Nature Neuroscience*, *9*(11), 1388–1396. https://doi.org/10.1038/nn1793

Vicini, S., Wang, J. F., Li, J. H., Zhu, W. J., Wang, Y. H., Luo, J. H., … Grayson, D. R. (1998). Functional and pharmacological differences between recombinant N-methyl-D-aspartate receptors. *Journal of Neurophysiology*, *79*(2), 555–66. https://doi.org/10.1016/0014-5793(92)80648-Z

Vyklicky, V., Korinek, M., Smejkalova, T., Balik, A., Krausova, B., Kaniakova, M., … Vyklicky, L. (2014). Structure, function, and pharmacology of NMDA receptor channels. *Physiological Research / Academia Scientiarum Bohemoslovaca*, *63 Suppl 1*, S191-203. Retrieved from http://www.ncbi.nlm.nih.gov/pubmed/24564659

Wadiche, J. I., Amara, S. G., & Kavanaugh, M. P. (1995). Ion fluxes associated with excitatory amino acid transport. *Neuron*, *15*(3), 721–728. https://doi.org/0896-6273(95)90159-0 [pii]

Wadiche, J. I., & Jahr, C. E. (2001). Multivesicular release at climbing fiber-Purkinje cell synapses. *Neuron*, *32*(2), 301–313. https://doi.org/10.1016/S0896-6273(01)00488-3

Watase, K., Hashimoto, K., Kano, M., Yamada, K., Watanabe, M., Inoue, Y., … Tanaka, K. (1998). Motor discoordination and increased susceptibility to cerebellar injury in GLAST mutant mice. *European Journal of Neuroscience*, *10*(3), 976–988. https://doi.org/10.1046/j.1460-9568.1998.00108.x

Wyllie, D. J., Mathie, A., Symonds, C. J., & Cull- Candy, S. G. (1991). Activation of glutamate receptors and glutamate uptake in identified macroglial cells in rat cerebellar cultures. *The Journal of Physiology*, *432*(1), 235–258. https://doi.org/10.1113/jphysiol.1991.sp018383

Yernool, D., Boudker, O., Jin, Y., & Gouaux, E. (2004). Structure of a glutamate transporter homologue from Pyrococcus horikoshii. *Nature*, *431*(7010), 811–818. https://doi.org/10.1038/nature03018

Zhou, Y., & Danbolt, N. C. (2013). GABA and Glutamate Transporters in Brain. *Frontiers in Endocrinology*, *4*(November), 1–14. https://doi.org/10.3389/fendo.2013.00165

Zhou, Y., & Danbolt, N. C. (2014). Glutamate as a neurotransmitter in the healthy brain. *Journal of Neural Transmission*. https://doi.org/10.1007/s00702-014-1180-8

APPENDIX

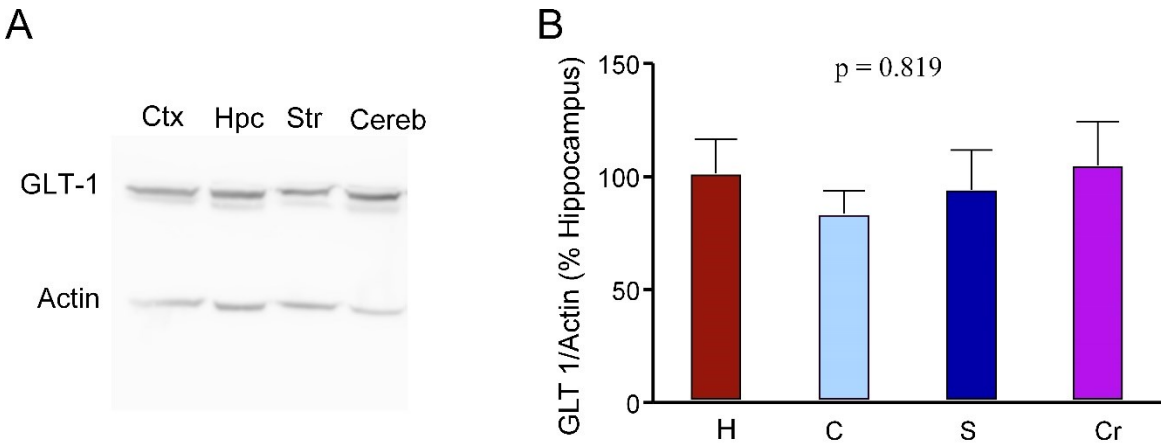

Figure A1**:** GLT-1 expression levels are similar in the adult hippocampus, cortex, striatum and cerebellum (Pinky et al., 2018). ***A***, Representative Western blot of GLT-1 expression in the cortex (Ctx), hippocampus (Hpc), striatum (Str) and cerebellum (Cereb). ***B***, Quantification of mean (±SEM) GLT-1 expression in the cortex (C), hippocampus (H), striatum (S) and cerebellum (Cr). ANOVA, *p*=0.819.